0 0 0 0 4 2 0 1 5 2 6

LBL-3176
c.1

PHASE TRANSFORMATIONS IN ORDERED, SPINODAL Cu-Mn-Al ALLOYS

Masuo Okada
(M.S. thesis)

October, 1974

Prepared for the U. S. Atomic Energy Commission
under Contract W-7405-ENG-48

For Reference

Not to be taken from this room

LAWRENCE BERKELEY LABORATORY
UNIVERSITY OF CALIFORNIA
BERKELEY

LBL-3176
c.1

DISCLAIMER

This document was prepared as an account of work sponsored by the United States Government. While this document is believed to contain correct information, neither the United States Government nor any agency thereof, nor the Regents of the University of California, nor any of their employees, makes any warranty, express or implied, or assumes any legal responsibility for the accuracy, completeness, or usefulness of any information, apparatus, product, or process disclosed, or represents that its use would not infringe privately owned rights. Reference herein to any specific commercial product, process, or service by its trade name, trademark, manufacturer, or otherwise, does not necessarily constitute or imply its endorsement, recommendation, or favoring by the United States Government or any agency thereof, or the Regents of the University of California. The views and opinions of authors expressed herein do not necessarily state or reflect those of the United States Government or any agency thereof or the Regents of the University of California.

0 0 0 0 4 2 0 1 6 2 7

PHASE TRANSFORMATIONS IN ORDERED, SPINODAL Cu-Mn-Al ALLOYS

Contents

Abstract v

I. Introduction 1

II. Experimental Procedures 4

A. Materials and Heat Treatment 4

B. Electron Microscopy 5

III. Results 6

A. "In Situ" Observation of Spinodal and Ordering Reactions . 6

1. Determination of the Miscibility Gap Temperature . . . 6

2. The Effect of Modulated Structure on APB Formation . . 9

B. Identification of the New Phase Appearing in Spinodally Transformed Cu-Al Rich Phase 11

1. Observation of the "New" Phase 11

2. Discussion of the Nature of the New Phase in the Cu-Al Rich Phase 13

3. Analysis of Diffraction Patterns 14

4. Crystal Orientation Relationships 15

5. Stability of the γ' Phase 16

IV. Discussion 18

A. Spinodal and Ordering Reactions 18

1. Determination of the Miscibility Gap 18

2. The Effect of Modulated Structures on APB Formation . 20

B. Identification of the New Phase Appearing in Spinodally Transformed Cu-Al Rich Phase 22

1. Classification of the $DO_3 \rightleftharpoons \gamma'$ Transformation (previously $DO_3 \rightleftharpoons L1_0$) 22

2. Metallography of the γ' Phase 27

3. γ' Phase and Spinodal Decomposition 29

V. Summary 31

Acknowledgements 33

Appendix. Calculation of the Values of the Extinction Distance (t_o) of Cu_3Al 34

References 36

Figure Captions 39

Figures 43

0 0 0 0 4 2 0 1 6 2 8

PHASE TRANSFORMATIONS IN ORDERED, SPINODAL Cu-Mn-Al ALLOYS

Masuo Okada

Inorganic Materials Research Division, Lawrence Berkeley Laboratory and Department of Materials Science and Engineering, College of Engineering; University of California, Berkeley, California 94720

ABSTRACT

Alloys along the composition line Cu_3Al-Cu_2MnAl decompose spinodally into a Cu_2MnAl rich phase and a Cu_3Al rich phase during aging at temperatures below 350°C. Hot stage electron microscopy was applied to determine the miscibility gap temperatures of the alloys by monitoring the disappearance of satellites in the diffraction mode and structure modulation in the image mode. The antiphase domain boundaries (APB's) developed during aging inside the miscibility gap were found to inherit the same character as those above the miscibility gap.

The new phase (the γ' phase) appearing in the spinodally decomposed Cu-Al rich phase was found to have an orthorhombic lattice with two layer stacking sequence (2H), which is considered to be formed by a shear along (110) planes of the parent β_1-lattice (DO_3). The Cu-12.4% Al-4.68% Mn alloy which is almost at the edge of the miscibility gap shows that slower quenching yields large amounts of γ' plates (martensite). This observation is in good agreement with that of the γ' phase in the Cu-Al rich phase, because the furnace cooled $Cu_{2.5}Mn_{0.5}Al$ alloy also gives a high density of γ' phase in the Cu-Al rich phase.

0 0 0 0 4 2 0 1 6 2 9

I. INTRODUCTION

Heusler[1] discovered a series of ferromagnetic alloys composed only of paramagnetic or diamagnetic elements. Although the relatively low saturation magnetization of these materials reported to date suggests that the alloys are not commercially attractive, the alloy having the highest saturation magnetization, namely Cu_2MnAl, has been rigorously investigated to elucidate the origin of its magnetic properties. There is also academic interest surrounding its phase transformation and precipitation behavior.

The metallography of the Cu-rich portion of the Cu-Mn-Al system at temperatures above 450°C, has been studied by West and Thomas.[2] Also the metallography of the alloys along the composition line Cu_3Al-Cu_2MnAl at temperatures below 350°C has been fully investigated by Bouchard and Thomas.[3-5] It is found that during decomposition along the Cu_3Al-Cu_2MnAl tie line, the system exhibits both ordering and spinodal reactions (Fig. 1).

The high temperature β phase, having a disordered bcc structure, orders rapidly during quenching. The ordering takes place in two stages, forming first a B2 structure, followed by a structure resembling an $L2_1$ or DO_3 superstructure (Fig. 2). During aging at temperatures below 350°C, the quenched structure decomposes and resulting microstructures show all the metallographic characteristics of spinodal decomposition, the theory for which has been developed in detail by Cahn[6] and Hilliard.[7] Low temperature aging also results in the appearance of extra reflections in selected area diffraction patterns. These extra spots have been indexed in terms of an $L1_0$ structure, which emerges within one of the

spinodal products, the Cu_3Al rich phase.

The determination of the spinodal temperature has been carried out in the Al-Zn system by using small angle X-ray diffraction.[8] A shortcoming of this and most other X-ray techniques, however, is the inability to produce a high resolution image of the (modulated) microstructures. Transmission electron microscopy enables a direct comparison of structure modulation and electron diffraction "satellite spots",[4,9] with the additional option of dynamic observation of phase transformations. Nevertheless, no work has been done so far on determining the miscibility gap by "in situ" experiments in the Cu-Mn-Al system (or any other spinodal).

Since the $(Cu\text{-}Mn)_3Al$ alloys decompose spinodally into a Cu_2MnAl rich phase and Cu_3Al rich phase during aging at temperatures below 350°C, this system is ideal for observing the spinodal reaction by "in situ" experiments with minor loss of image quality due to thermal instabilities. One objective of this investigation is to determine the miscibility gap temperature of $(Cu\text{-}Mn)_3Al$ by monitoring the disapperance of satellites in the diffraction mode and structure modulations in the image as a function of aging temperature. This technique will also facilitate an estimation of the spinodal temperatures. Because spinodal and ordering reactions occur simultaneously in these alloys, this system also lends itself well to an investigation of the interactions between structure modulations and APB's (anti-phase domain boundaries), which will be also discussed in the light of hot-stage electron microscope experiments.

The mechanical behavior of spinodally decomposed and aged alloys has been investigated by several workers.[9-12] The structure and mechanical properties of the $Cu_{2.5}Mn_{0.5}Al$ alloy, which lies at the center of the miscibility gap along the Cu_3Al-Cu_2MnAl pseudo-binary have also been studied.[13] Because of the extensive brittleness of the alloy, Vicker's hardness test was adopted to indicate the variation in strength with aging. These results reveal that a new phase tentatively identified as having an $L1_0$ structure, plays an important role in increasing the Vicker's hardness. It is, therefore, important to classify the transformation $DO_3 \rightleftharpoons L1_0$. One possible mechanism of the transformation was proposed by Bouchard and Thomas.[4] However, the stability of the $L1_0$ phase is still unsolved.

In this paper other possibilities of the $DO_3 \rightleftharpoons L1_0$ transformation will be discussed with respect to a martensitic transformation, since the composition of the original DO_3 structure is Cu_3Al, a known candidate for a martensitic reaction. The stability temperature of the $L1_0$ phase is estimated by hot-stage electron microscopy and the metallography of the $L1_0$ phase is re-examined by high resolution dark field techniques.

II. EXPERIMENTAL PROCEDURES

A. Materials and Heat Treatment

Three alloys were chosen to determine the miscibility gap temperature. Table I shows the compositions of the alloys studied.

Table I. Atomic and chemical compositions of the alloys studied.

Atomic Composition	Estimated Composition		
	Wt% Cu	Wt% Mn	Wt% Al
$Cu_{2.8}Mn_{0.2}Al$	82.5	5.1	12.5
$Cu_{2.5}Mn_{0.5}Al$	74.4	13.1	12.5
$Cu_{2.2}Mn_{0.8}Al$	66.3	20.8	12.8

The alloys were prepared from 99.999% Cu, 99.9% Mn and 99.999% Al by arc melting in helium atmosphere and were chill cast into a copper mold. Chemical analysis verified to within 1% the compositions given previously.

The ingots were then placed in stainless steel envelopes, homogenized for 3 days at 850°C and oil quenched in order to avoid quenching cracks. Thin slices, 0.5 mm thick, were the cut and homogenized at 850°C for 10 min under argon atmosphere in a vertical resistance furnace. Thin slices for determining the temperature of the miscibility gap were then quenched in an oil bath to develop a particular spinodal wavelength.

Samples for identifying the structure of the so called $L1_0$ phase were furnace cooled because this treatment was found to produce well

defined $L1_0$ reflections.[13]

Specimens aged for 1000 min at 275°C in salt baths (50% potassium nitrate, 50% sodium nitrate) were also examined for comparison.

B. Electron Microscopy

Electron microscope disc specimens, 3.0 mm in diameter were spark eroded, followed by thinning in an automatic jet polisher using an electrolytic solution of 400 ml acetic acid, 20 ml water, 75 gr chromic oxide.

All "in situ" observations were made using a goniometer heating-holder in a Philips EM301 electron microscope. Photomicrographs were taken at temperature after the image had ceased drifting, using a short exposure time to avoid blurring. The hot stage was calibrated by the temperature at which a cobalt foil was observed to transform from hcp to fcc on increasing the temperature. At 450°C the microstructure consists of approximately 50% hcp and 50% fcc phase. The accuracy of the temperature given here is estimated to be better than ±5°C.

A high-angle tilt goniometer stage was used for determining the structure of the new phase transformed from the DO_3 structure. The stability of this phase was also investigated using hot-stage analysis.

III. RESULTS

A. "In Situ" Observation of Spinodal and Ordering Reactions

1. Determination of the Miscibility Gap Temperature

On heating specimens from room temperature, crossing the spinodal limit results not only in the disappearance of satellites but also in the resolution of the characteristic spinodal structure modulations. Although the disappearance of the satellites can also be attributed to loss of coherency of the spinodal product, there are other diffraction effects which distinguish the break of coherency. These effects include the splitting of diffraction spots in a direction parallel to each reciprocal lattice vector g. A further indication of loss of coherency is the generation of interfacial dislocations as a typical morphology. In the $Cu_{2.5}Mn_{0.5}Al$ alloy, the loss of coherency occurs after aging at 300°C for approximately 1,000 min,[13] and these conditions far exceed those employed in the present study. In addition, neither diffraction spot splitting nor the presence of interfacial dislocations was observed, hence coherency of the spinodal product is apparently maintained throughout "in situ" heating.

The temperature of the miscibility gap was determined by monitoring the disappearance of satellites and of modulated microstructures. The spinodal wavelengths were calculated from the satellite spacings in selected area diffraction patterns, and by direct measurements from the photographs. The former method is more accurate as it is independent of optical magnification. The closer the specimen temperature is to the miscibility gap temperature, the smaller the satellite spacing becomes.[6] For longer wavelengths

(i.e., over 130 Å) a microdensitometer analysis was also carried out on photographically enlarged diffraction patterns to detect the satellite spots around the Bragg reflections.

Foils were oriented in an [001] direction to optimize detection of the changes of modulated structures and satellites around the (200) reflections. A temperature sequence of micrographs is shown in Fig. 3 for the asymmetrical alloy, $Cu_{2.2}Mn_{0.8}Al$. The imaging conditions for the best detection of the changes of modulated structures were utilized, and these are shown in the corresponding diffraction patterns of Fig. 4, which also depict changes in the satellites about the (200) reflection. The images show some contamination but the typical modulation contrast is clearly resolved at temperatures above 273°C in the sequence of Fig. 3.

During heating of the foil, well defined satellites are observed to develop from the original diffuse satellites. This is believed to arise from the preferential growth of a critical compositional wavelength along the elastically soft cubic directions from the range of initial wavelengths.[6] The satellite spacing decreases with increasing temperature. In an asymmetrical alloy, the satellites are asymmetrical in intensity consistent with the volume fraction of Cu_3Al being lower than that of the major phase, Cu_2MnAl.

Below 307°C, well defined satellites were observed, but at 318°C, all reflections were streaked in a direction parallel to ⟨100⟩. Therefore, no measurement of the wavelength was made above 318°C from diffraction patterns. Micrographs reveal that the minor phase forms as thin platelets parallel to the cube planes of the matrix. This

suggests that the streaks in the associated diffraction pattern can be explained by the shape factor effect of these observed plate-like particles which produce rel-rods in a direction normal to the plate habit planes. Since above 318°C, no satellites were observed in the diffraction patterns, but composition modulations were seen in bright field images, it follows that 318°C lies inside the miscibility gap but outside the spinodal. Diffraction spot streaking dissappeared at 328°C, but in the corresponding micrographs, the plate-like precipitates were not completely dissolved. The temperature of the miscibility gap is believed to be around 358°C, since this temperature corresponds to the complete dissolution of the plate-like precipitates in the bright field micrographs. A similar sequence of pictures was taken of the $Cu_{2.5}Mn_{0.5}Al$ alloy and the temperature of the miscibility gap was determined as 350°C±5°C, by monitoring the dissolution of the modulated structures. However, for this alloy the temperature at which the modulated structure dissolved very nearly coincided with that of the disappearance of satellites. Therefore, the temperature of the miscibility gap, 350°C±5°C, for the $Cu_{2.5}Mn_{0.5}Al$ alloy, is believed to be close to the spinodal temperature.

These results are summarized in Fig. 1 showing the limits of the miscibility gap, which are in good agreement with the previous results obtained by studying the constituents of the microstructures obtained after prolonged aging when the coarsening process has taken place.[3]

2. The Effect of Modulated Structure on APB Formation

There are two possible types of APB vectors in both the DO_3 and $L2_1$ structures, a/4⟨111⟩ and a/2⟨100⟩. The following table gives the phase change angle $\alpha = 2\pi(\vec{g}\cdot\vec{R})$ associated with phase contrast due to the presence of both types of APB's ($\vec{g}$ is the operating reflection and $\vec{R}$ is the anti-phase vector) and the values of extinction distances of Cu_2MnAl and Cu_3Al, which are estimated by Marcinkowski[14] and in this paper (see Appendix), respectively. There is no contrast when $\alpha = 0$ or $n\cdot 2\pi$ and few fringes are obtained when t_o is large.

Table II. Antiphase angle and extinction distances of the DO_3 and $L2_1$ type superstructures.

hkl	Type of Reflection	α for 1/4a⟨111⟩	α for 1/2a⟨100⟩	t_o in Cu_2MnAl (Å)	t_o in Cu_3Al (Å)
111	S_I	±π/2	±π	2,700	3,160
200	S_{II}	±π	0	1,680	3,415
220	F	0	0	308	590

Referring to Table II, it is apparent that S_I type reflections give contrast for 1/4a⟨111⟩ and 1/2a⟨100⟩ APB's, but that with S_{II} type reflections, only the 1/4a⟨111⟩ APB's can be imaged. The energies of the two types of APB's in the DO_3 structure are small and nearly isotropic.[14] No such calculations have been made for the $L2_1$ structure but in view of the similarities with the DO_3 structure, the APB energies for the $L2_1$ structure are also expected to be small. The extinction distances for S_I and S_{II} type reflections are large in comparison with foil thickness (i.e., 1000 Å), so that the contrast of an APB at s = 0 (where s is the deviation parameter) in Cu_2MnAl

and Cu_3Al would consist of a single broad band with a contrast comparable to that observed in Fe_3Al.[15]

One of the necessary conditions of a system to undergo spinodal decomposition is that the structure of the two decomposed phases be nearly identical, in order to allow continuity in modulation. In the case of ordered structures, therefore, the types of APB of the decomposed two phases are expected to be nearly the same. If the extinction distances of the superlattice reflections for the two phases have the same value, the images of the APB's would be continuous through the decomposed two phases.

In previous work,[3] it is reported that the APB's of the as-quenched alloys remained smoothly curved during brief aging at temperatures well inside the miscribility gap even though the microstructure is modulated. Figure 5(a) is a good example of this behavior. To enquire how APB's would behave when the specimen temperature exceeds that of the miscibility gap, hot stage sequences of the (111) dark field micrographs shown in Fig. 5 were taken of the $Cu_{2.5}Mn_{0.5}Al$ alloy. The foil was oriented in a [110] zone where composition modulations parallel to [100] are imaged, along with the isotropic APB's. There APB's were shown to be of the type a/2⟨100⟩ by taking a (200) dark field micrograph, in which no APB's were seen (See Table II). It should be noted that the 1/4a⟨111⟩ APB's generated at T_c(B2) (750°C for $Cu_{2.5}Mn_{0.5}Al$) have a higher energy than the 1/2a⟨100⟩ APB's generated at $T_c(L2_1\text{-}DO_3)$ (600°C for $Cu_{2.5}Mn_{0.5}Al$). Therefore, it remains a possibility that 1/4a⟨111⟩ APB's exist within this structure, but, due to a large domain size, they lie outside the field of view of the micrographs in Fig. 5.

The [100] composition modulations lose contrast at 357°C (Fig. 5(d)), whereas the antiphase domain size increases as the temperature is increased. This observation indicates that the APB's developed during aging inside the miscibility gap inherit the same character above the miscibility gap. It is, therefore, believed that there is little interaction between the APB's and modulated structure. This observation can be explained on the basis of the reasons mentioned before; viz, (1) the types of APB's of the decomposed phases are the same as that of the ordered solid solution found above the miscibility gap, and (2) the APB energies in these structures are nearly isotropic. In addition, since this research relies on transmission electron microscopy, it is necessary that the imaging characteristics of the APB's be known, particularly any differences due to phase transformations. This problem is eliminated in the present study due to the similarity of the (111) extinction distances for the Cu_2MnAl and Cu_3Al phases and the $L2_1$-DO_3 solid solution.

B. Identification of the New Phase Appearing in Spinodally Transformed Cu-Al Rich Phase

1. Observation of the "New" Phase

The general morphology of the new phase has been reported previously,[4,13] and in this paper its structure is reconsidered. The new phases are imaged in one of the spinodally decomposed products, which was shown to be the Cu_3Al rich-phase by Bouchard and Thomas.[4]

Figure 6(a) taken from the furnace cooled $Cu_{2.5}Mn_{0.5}Al$ alloy reveals the modulated structure, with a wavelength of 210 Å. The corresponding diffraction pattern is shown in Fig. 7.

A dark field micrograph of the same area is shown in Fig. 6(b), obtained using the extra reflections marked N due to the new phase. The image shows that each small particle is elongated parallel to ⟨111⟩ which is the trace of {110} planes. The analysis of the morphology will be explained later. Figure 6(c) is a dark field micrograph using the diffraction spot marked M in Fig. 7. The random distribution of the particles having various sizes indicates that the reflection M is not simply due to a transformation in either Cu_3Al-rich phase or in Cu_2MnAl-rich phase, but is due to contamination, as demonstrated later.

The (310) micrograph taken from the aged specimen for 1000 min at 275°C shown in Fig. 8(a) is another example clearly imaging the new phase as black particles (B.F.) within the Cu_3Al rich phase. The micrograph clearly shows that the new phase is imbedded in the Cu_3Al phase and results from partial transformation of the DO_3 structure. The dark field micrograph of the new phase shown in Fig. 8(b) was obtained using the spot marked N in Fig. 9. The long axes of the imaged small particles are for the most part parallel to ⟨133⟩, which is also a trace of {011} planes as seen in Fig. 6(a) and (b). The dark field micrograph of Fig. 8(c) imaged with the reflection marked M in Fig. 9 illustrates that the small particles are dispersed throughout the area of the specimen, which is consistent with the morphology shown in Fig. 6(c).

2. Discussion of the Nature of the New Phase in the Cu-Al Rich Phase

It is well known that in binary Cu-Al alloys, Cu_3Al transforms martensitically to the 9R structure.[15] The martensites are produced by a shear along one of the ⟨110⟩ planes of the parent β_1 phase (DO_3 type), whose crystal structure consists of alternate stacking layers parallel to the (110) plane, as shown in Fig. 10(b). The structure of the Cu-Al martensite varies with the Al content as shown in Table III below:

Table III.* Cu-Al martensite.[16-18]

Wt% Al	Symbol	Structure	Ms Temperature
11 Al	β'	fcc	450°C
11~13 Al	β_1'	9R	450°C~240°C
13~15 Al	γ'	2H	240°C

*β_1' martensite is an ordered orthorhombic lattice consisting of units of 18 close-packed layers (9R) along the C direction. (AB'CB'CA'CA'BA'BC'BC'AC'AB'). γ' martensite consists of units of two close packed layers AB'(2H) (see References 17 and 18).

It is possible that the new phase appearing in the Cu_3Al rich phase of the ternary Cu-Mn-Al alloys examined here would have this martensitic character. However, in the early stage of spinodal decomposition, the Cu_3Al rich component of the spinodal produce will contain Mn, which might have an effect on any subsequent transformation. It is reported that the structure of the martensite of Cu-12.5 wt% Al-4 wt% Mn alloy is based on an orthorhombic unit cell (2H structure).[19] Upon analyzing more diffraction patterns, the possibilities of those structures mentioned above were taken into consideration.

3. Analysis of Diffraction Patterns

A series of diffraction patterns representing several sections of reciprocal space (e.g., Figs. 7, 9, 20) was taken to determine the structure of the new phase. The result was best described by an orthorhombic structure, whose atom coordinates in the unit structure cell illustrated in Fig. 10(b) are:

Al	Cu or Mn	
(000)	$\left(0,\frac{1}{2},0\right)$	$\left(\frac{1}{3},0,\frac{1}{2}\right)$
$\left(\frac{1}{3},\frac{1}{2},\frac{1}{2}\right)$	$\left(\frac{1}{2},\frac{1}{4},0\right)$	$\left(\frac{5}{6},\frac{1}{4},\frac{1}{2}\right)$
	$\left(\frac{1}{2},\frac{3}{4},0\right)$	$\left(\frac{5}{6},\frac{3}{4},\frac{1}{2}\right)$

The structure consists of two close-packed layers AB' (fundamentally a hexagonal close-packed structure), which is identical to the γ' phase in binary Cu-13~15% Al alloys[17] and Cu-12.5 wt% Al-4 wt% Mn alloys,[19] so it will also be called γ' by comparison. The reflections from the γ' phase and the Cu_2MnAl phase often superimpose, so that it is very difficult to uniquely determine the lattice parameter of the γ' phase. But the bright field shown in Fig. 8(a) illustrates that the γ' phase may be coherently imbedded in the Cu_3Al-rich phase. The lattice parameters of the γ' phase estimated from the Cu_3Al matrix unit cell are:

$A^* = 4.12$ Å
$B^* = 5.84$ Å
$C^* = 4.03$ Å

Plane sections of the reciprocal lattice of the γ' phase are given in Fig. 11. Relative intensities are also indicated (from structure factor amplitudes only).

4. Crystal Orientation Relationships

One way to determine an orientation relationship is to compare observed interplanar angles between a pair of planes of the matrix and the γ' phase with those expected from the assumed orientation relationships for a number of pairs of planes. For indexing matrix reflections with respect to γ' reflections in order to determine the orientation relationship, the following specific lattice correspondence was always taken:

$$\left[\tfrac{1}{2}\ \tfrac{1}{2}\ 0\right]_{\beta_1} \rightarrow [100]_{\gamma'}$$

$$[0\ 0\ \bar{1}]_{\beta_1} \rightarrow [010]_{\gamma'}$$

$$\left[\tfrac{1}{2}\ \tfrac{1}{2}\ 0\right]_{\beta_1} \rightarrow [001]_{\gamma'}$$

Because of the weak intensity of the γ' reflection, the orientation relationship is not determined definitely. According to the proposed γ' structure, the $(110)_{\beta_1}$ plane corresponds to the $(001)_{\gamma'}$ plane. The dark field micrograph of the γ' phase shown in Fig. 6(b) illustrates the basal plane orientation. As discussed before, the small particles are elongated parallel to $[1\bar{1}\bar{1}]_{\beta_1}$ and $[1\bar{1}1]_{\beta_1}$ directions. In corresponding diffraction patterns, the diffuse streaks lie in $[1\bar{1}\bar{2}]_{\beta_1}$ and $[112]_{\beta_1}$ The stereographic projection shown in Fig. 12 indicates the correlation between the elongated particles and the origin of the diffuse streaks in the diffraction pattern. In the stereographic projection, marks □ correspond to the matrix β_1 ordered phase, marks • indicate those of γ' expected from the assumption that $(110)_{\beta_1} \parallel (001)_{\gamma'}$, $[1\bar{1}1]_{\beta_1} \parallel [2\bar{1}0]_{\gamma'}$ and marks ○ specify those when another relationship is assumed to be $(110)_{\beta_1} \parallel (001)_{\gamma'}$, $[\bar{1}11]_{\beta_1} \parallel [\bar{2}\bar{1}0]_{\gamma'}$

Assuming that $(110)_{\beta_1} \parallel (001)_{\gamma'}$ and $[1\bar{1}1]_{\beta_1} \parallel [2\bar{1}0]_{\gamma'}$ hold, the direction of the streaks, $[1\bar{1}2]$, is normal to the $[1\bar{1}\bar{1}]_{\beta_1}$ direction in which the γ' particles are lengthened and is the trace of the $(121)_\gamma$ or $(\bar{1}\bar{2}1)_\gamma$ plane. However, identical diffraction effects will result for the alternative relationship, $(110)_{\beta_1} \parallel (001)_{\gamma'}$, , $[\bar{1}11]_{\beta_1} \parallel [\bar{2}\bar{1}0]_{\gamma'}$ Experimentally it is very difficult to distinguish which relationship is more probable because of the diffuseness of the γ' spots.

5. Stability of the γ' Phase

The stability of the γ' phase was studied by heating the foil in the the microscope. Furnace cooled specimens were chosen for heat treatment because of their high density of the γ' phase, as reported previously.[13]

In Fig. 13, the sequence of dark field micrographs was obtained with the γ' reflections marked as γ' in the corresponding diffraction patterns shown in Fig. 14. Figure 14(a) shows the regular array of fine particles of the γ' phase within the Cu_3Al rich phase as in Fig. 6(b). The corresponding diffraction pattern given in Fig. 14(a) indicates that in addition to the γ' spots, the extra spots marked M are formed. At 157°C, the particles begin to be imaged poorly in the dark field micrograph, but the reflections due to the phase are still present. They disappeared at 205°C. This indicates that the reversion temperature of the γ' phase developed during furnace cooling is around 205°C.

At higher temperature, 222°C, a diffuse ring pattern is formed along the M spots and the intensity of the M spots seem to increase. The dark field of the M spots is shown in Fig. 15(g), which shows that the small particles are distributed over all the thin specimen. At 400°C, the equilibrium phases in this alloy are; Cu_3Mn_2Al, γ and β_{Mn}.[2]

The precipitation of these phases can be suppressed by quenching. However, it has been reported that precipitation of the equilibrium phase may occur due to electron bombardment in the electron microscope as in the Cu-Sn system.[20]

In the present investigation, no evidences of the presence of β_{Mn} and Cu_3Mn_2Al were found. The M spots appearing in (110) (as shown in Fig. 7) and (112) (not shown in this paper) diffraction patterns closely fit the lattice parameters of the γ phase, but those in the (001) pattern did not. A further indication of the origin of the M spots was made by observing a thin specimen kept in air for two months at room temperature after being bombarded by electrons in the microscope. Figures 15(a), (b) and (c) were taken of the old specimen. In Fig. 15(c), strong M spots are observed, but the reflections due to the γ' phase are absent. This substantiates the suggestion that M apots are due to some sort of contamination e.g., oxidation or phase transformation occurring characteristically in thin specimens at room temperature, because a bulk specimen kept in air for two months at room temperatures does not give M spots at all. Since the lattice spacings corresponding to the M spots are not found in the Cu or Mn or Al oxides listed in ASTM cards, M spots may arise from not merely simple one element oxides, but rather from complex two or three element oxides. More work is needed to establish the origin of M spots.

IV. DISCUSSION

A. Spinodal and Ordering Reactions

1. Determination of the Miscibility Gap

The dissolution at the higher temperature of a structure developed by aging at a lower temperature would possibly occur for one of the following three cases;[7] (1) the reversion temperature is within the coherent spinodal, (2) the reversion temperature is above the coherent spinodal but within the metastable region and (3) the reversion temperature is above the coherent phase boundary. Because there are apparently no experimental elastic constants and thermodynamic data available for the Cu-Mn-Al ordered solid solution, the coherent spinodal, which allows for the stablizing effect of elastic energy on coherency strains, is not able to be estimated. However, the chemical spinodal curve can be calculated from the formula derived by Cook and Hilliard.[21]

$$C_s - C_c \simeq C_e - C_c[1-0.422(T/T_c)] \quad .$$

C_s and C_e are the spinodal and equilibrium compositions at temperature T, and C_c is the critical compositions at the critical temperature T_c. Using $T_c \sim 355°C$ and $C_c \sim 0.65$, which values were adopted from the estimated miscibility gap curve, the chemical spinodal is derived (Fig. 1).

The limits of the miscibility gap illustrated in Fig. 1 were obtained by monitoring the disappearance of satellites and of modulated structures. For the $Cu_{2.2}Mn_{0.8}Al$ alloy, the temperature at which the satellites were not detectable even by a microdensitometer analysis, was not consistent

with that at which the modulated structure was dissolved. But for the $Cu_{2.5}Mn_{0.5}Al$ alloy, both temperatures were very close together. This finding might be explained by referring to Fig. 1 showing the limits of the miscibility gap and the chemical spinodal curves. For the $Cu_{2.2}Mn_{0.8}Al$ alloy, the satellites dissapeared and all reflections were streaked in a direction parallel to ⟨100⟩, as shown in Fig. 3(b), at 318°C, which is close to the temperature of the estimated chemical spinodal (310°C). From the bright field micrograph at 318°C, the wavelength λ was estimated to be ~230Å, the corresponding satellites of which should have been detected in the diffraction pattern since satellites spacings of wavelength less than ~300Å were measurable. Instead of the satellites, streaks were observed. This observation suggests that the spinodal temperature for the $Cu_{2.2}Mn_{0.8}Al$ alloy is around 318°C. For the $Cu_{2.5}Mn_{0.5}Al$ alloy the difference between the temperature of the miscibility gap and the chemical spinodal temperature is ~14°C. This may explain why the satellites and the modulated structure dissapeared nearly at the same temperature for the $Cu_{2.5}Mn_{0.5}Al$ alloys.

Because the misfit between the coherent particles in this system is large (~2%), the coherent spinodal is expected to be depressed below the chemical spinodal. However, as an example, the $Cu_{2.5}Mn_{0.5}Al$ alloy is very brittle as shown by the tensile date reported previously.[13] Young's modulus estimated from the stress-linear strain curve is $\sim 5\times10^{8}$ (dyn/cm^2) ($Y_{(100)}$ Cu ~ 1.15×10^{12} dyn/cm^2), assuming the deformation occurred not along the grain boundary but uniformly within the grain. It should be noted that the estimation of Young's modulus made here is subject to a great uncertainty since the polycrystal specimens are

surely deformed along the grain boundary regions. If Young's modulus is very small, a strain energy term $\eta^2 Y$, in which $\eta = (1/a)\ (da/dc)$ and Y is Young's modulus, is also small. Therefore the coherent spinodal, given by the locus of $f'' + 2\eta^2 Y = 0$, may be in approximately the same position as the chemical spinodal. As discussed above, metallographic features on heating the system are well explained by the position of the chemical spinodal, which also suggests that the coherent spinodal and the chemical spinodal coincide.

2. The Effect of Modulated Structures on APB Formation

Morral and Cahn[22] extend the theory of spinodal decomposition to ternary systems and show the possibility of spinodal decomposition and continuous ordering occurring simultaneously. Also, in binary systems, it has been reported that Fe-Be alloys decompose into a periodic, modulated structure containing Fe-Be particles with the ordering CsCl structure.[23-25] M. J. Richards and J. W. Cahn[26] examined the ground state energy and superstructures of bcc and fcc using Ising model systems by taking account of second neighbor interactions and demonstrated that ordering and clustering are not mutually exclusive even for binary alloys.

One of their results is illustrated in Fig. 16 to show the curve of the energy of mixing of various states as a function of composition, where first and second neighbor interaction parameters, V_1 and V_2 are positive and $4/3 > V_2/V_1 > 2/3$. The ordered structure in the ground state up to 25% (and between 75 and 100%) is of the Fe_3Al(Fm3m) type. There are two superstructures that are candidates for the ground state between 25 and 50% B; (a) a superstructure with symmetry Fm3m and 16 atoms per cell with sites in position II of the Fe_3Al lattice (DO_3 structure)

being progressively filled by B; (b) a superstructure with the lower symmetry of space group $F\bar{4}3m$ and 16 atoms per unit cell, with sites either in position I or III being progressively filled by B.

By extending this idea to the pseudo-binary phase diagram composition along the Cu_3Al-Cu_2MnAl alloy shown in Fig. 1, Fig. 16 indicates the possible metastable transition phases that might form during transformation from the disordered state to the equilibrium state following a quench from high temperatures. Figure 16 is well followed by the sequence of ordering reactions occurring in the alloys along the composition line Cu_3Al-Cu_2MnAl. Referring to Fig. 1 and Fig. 2, a disordered bcc structure first orders to a B2 structure and further orders to a DO_3-$L2_1$ structure. The non-stoichiometric superstructure up to 25% Mn would form the superstructure resembling an $L2_1$ structure because excess Mn atoms favor type II sites in place of Cu atoms according to Fig. 16 showing Fm3m in the ground state. On the Cu_2MnAl side (between 75 and 100% Mn), excess Cu atoms tend to replace type II sites instead of Mn atoms. Thus DO_3-$L2_1$ structures are stabilized through the composition line Cu_3Al-Cu_2MnAl above a certain temperature. The DO_3-$L2_1$ structure is in the ground state up to 25% Mn (and between 75 and 100 Mn), so that the superstructure is relatively stable at lower temperature near these compositions (below 350°C). The superstructure in the ground state between 25 and 50% is space group $F\bar{4}3m$.

From the symmetry of the curve in Fig. 16, the same arguments hold also between 45 and 100% B. Excess Mn atoms in the Cu_3Al alloy progressively fill up positions I or III rather than position II shown in Fig. 2. For

the Cu_2MnAl side in this range (between 50 and 75% Mn), Cu atoms are in excess and Mn atoms are deficient with respect to the $L2_1$ structure. These excess Cu Atoms may diffuse to the Cu_3Al phase to form the nearly stoichiometric crystal (DO_3) and further reduce the energy of mixing. On the other hand, the excess Mn atoms in the Cu_3Al phase may tend to diffuse to form the nearly stoichiometric $L2_1$ structure. This may explain the origin of Cu rich or Mn rich sinusoidul compositional modulations which develop inside the miscibility gap. However, it is uncertain whether the superstructure within the miscibility gap possesses the Fm3m or the $F\bar{4}3m$ space group symmetry. X-ray diffraction techniques cannot be used to experimentally distinguish between these two superstructures. Even if the superstructure within the miscibility gap is $F\bar{4}3m$, it is expected that the APB configuration of $F\bar{4}3m$ is the same as that of Fm3m (DO_3). This model supports the observation that APB's developed during aging inside miscibility gap inherit the same character above the miscibility gap.

B. Identification of the New Phase Appearing in Spinodally Transformed Cu-Al Rich Phase

1. Classification of the $DO_3 \rightleftharpoons \gamma'$ Transformation (previously $DO_3 \rightleftharpoons L1_0$)[4,13]

It was reported that a slower quench results in the appearance of a new phase (γ') in the Cu_3Al rich phase. Increasing the quench rate decreases the amount of the new phase.[13] This observation can be explained by the character of a thermoelastic martensite expected in Cu-Al based alloys.

The martensite which emerges in an Fe-30% Ni alloy is normally formed by a high degree of undercooling, but thermoelastic martensite

(e.g. Au-47.5% Cd) requires little driving force for the transformation to occur.[27] The conventional martensite transforms by "bursting" to a final size at a high under-cooling, but thermoelastic martensite grows in length and width with cooling. There is also significant differences in As (austenite start temperature) and Ms (martensite start temperature) between conventional and thermoelastic martensites. The difference between As and Ms is large (400°C for the Fe-30% Ni alloy) in the former case, but is small (15°C for Au-47.5% Cd) in the latter case.[27]

As shown in Table 2, the Ms temperature of the γ' phase appearing in the Cu-Al system is 240°C or below and decreases with the increasing Al content. The Ms temperature of the γ' phase in the Cu-Al system is in quite good agreement with the reversion temperature of the γ' phase (205°C), estimated from the furnace cooled specimen ($Cu_{2.5}Mn_{0.5}Al$) by hot stage analysis. Because it is expected that the difference between Ms and As is very small for thermoelastic martensite, the Ms temperature of the γ' phase in the Cu_3Al rich phase would be close to the reversion temperature of the γ' phase.

However, in an early stage of spinodal decomposition, one of the spinodal products, the Cu_3Al rich phase, will contain some amount of Mn. The effects of Mn addition on the phase transformation of the β Cu-Al alloys have been investigated by several workers.[19,28]

Tarora[28] reported that Mn additions depress the temperature of eutectoid decomposition $\beta \rightarrow \alpha + \gamma_2$ and tend to suppress the occurrence of the decomposition. The Ms temperature of the $\beta_1 \rightarrow \beta_1'$ transformation is also lowered by the addition of Mn and Al. Sugino, Nakanishi and Mitani[19] also studied the effects of Mn addition on martensite in Cu-Al

alloys by means of specific heat and X-ray measurements. It was found that two types of martensite, β_1' and γ', were formed in a Cu-11.8% Al-4% Mn alloy. After iced brine quenching, only the β_1' martensite peak was detected around 385°C on specific heat vs temperature curves for the alloy. But in slowly cooled specimens (i.e., a furnace cool or an air cool), a martensite peak was found at 170°C in addition to the β_1' martensite. As the quenching rate is reduced, the peak corresponding to γ' martensite becomes stronger and the β_1' peak becomes weaker.

As shown in Table III, increasing the Al content varies the structure of the martensite in the Cu-Al system. In the Cu-Al-Mn system, the structure of the martensite is additionally subject to heat-treatment, as well as composition variations. Figures 17, 18 and 19 were taken from Cu-12.4% Al-4.68% Mn alloy which is almost at the end of miscibility gap for the Cu_3Al rich phase. The former two specimens were oil quenched and the latter one was furnace cooled. Oil quenching yields the ordered β_1 single phase as shown in Fig. 17, although some areas contain the twinning plates shown in Fig. 18. Furnace cooling produces a plate-like morphology, having internal striations. The diffraction pattern shown in Fig. 19(a) was taken from the plate marked (a) in the bright field micrograph. The structure of the plate found here is analysed to be identical with that of the γ' phase in the Cu_3Al rich phase. The direction of strong streaking in the diffraction pattern is perpendicular to the direction of the striations in the bright field micrograph, so that the striations are due to a high density of stacking faults. The striations in the plate marked (b) are normal to

those in the plate marked (a). The diffraction pattern taken from the area marked C, including both plates (a) and (b), gives the same pattern as that taken from the furnace cooled $Cu_{2.5}Mn_{0.5}Al$ alloy shown in Fig. 20. The (001) diffraction pattern of the furnace cooled $Cu_{2.5}Mn_{0.5}Al$ alloy is indexed in terms of the two variants of the γ' phase. The morphology of the two variants of the γ' phase in an (001) orientation has been discussed extensively in previous papers.[4,13]

The density of plates observed in Fig. 19 increases with decreasing quenching rate. This implies that the plates are formed from the ordered β_1 phase because slower quenching results in developing a higher degree of ordering. Cahn and Coll[29] confirmed that an Fe_3Al alloy with the DO_3 type structure shows resistance to twinning if the degree of order is increased, and that the alloy does not exhibit twinning if it is fully ordered. This is consistant with the observation made here.

Since those plates (possibly the α' martensite) emerging in the Cu-12.4% Al-4.68% Mn alloy obey the observed α' phase behavior in the Cu_3Al righ phase, and since the alloy is located near the Cu_3Al rich side of the miscibility gap, the γ' martensite in Cu-12.4% Al-4.68% Mn may have the same origin as the γ' phase in the Cu_3Al rich material.

The structure of this new phase (γ') was previously proposed[4] to be of the $L1_0$ type, which is generated from the DO_3 structure by the partial disordering of the DO_3 lattice to the B2 lattice, followed by the ordering of only one set of the {110} planes of the B2 structure. However, this mechanism would fail to explain the observation that the amount of the $L1_0$ phase increases with decreasing quenching rate, on

the basis of the arguments which follow:

(1) The proposed mechanism involves the generation of non-conservative APB's of the DO_3 structure parallel to every (220) plane of the structure.

(2) The surface energies of non-conservative APB's will be higher relative to conservative APB's due to the change in local composition across non-conservative

(3) The APB energy of both types are also proportional to S^2 where S is the degree of long range order. Consequently the relative difference in energies will be small in partially ordered alloys and may effectively vanish in as-quenched alloys. This implies that conservative APB's are more stable than non-conservative APB's when the degree of order, represented by S, is high.

Therefore, it is expected that iced-brine quenched alloys would produce a high density of the $L1_0$ phase due to the stabilization of non-conservative APB's which is required for the nucleation of the $L1_0$ phase. Slowly quenched alloys would have a lower density of the $L1_0$ phase due to destabilization of the non-conservative APB's (S is large).

The experimental observations, however, are inconsistent with the prediction made above, based on the previously proposed mechanism. Instead, the origin of the γ' phase is proposed in this paper to be the transformation of the ordered DO_3 phase, by homogeneous $\langle 110 \rangle$ shear, to an orthorhombic Cu_3Ti type structure shown in Fig. 10, which is similar to the γ' martensite in Cu-Al-Mn (or in Cu-Al).

2. Metallography of the γ' Phase

The structure of the γ' phase in the Cu_3Al rich phase was determined to be orthorhombic, with lattice parameters of A = 4.12Å, B = 5.84Å and C = 4.03Å. However, the lattice parameters of the γ' phase in Cu-12.5% Al-4% Mn and in Cu-13% Al, have been reported to be a = 4.45Å, b = 5.30Å, c = 4.24Å[19] and a = 4.51Å, b = 5.20Å, c = 4.22Å,[17] respectively. It is considered that the γ' martensite in the Cu-Al system is formed by a shear along (110) planes of the parent β_1-lattice, accompanied by shuffling on alternate layers. But the Cu_3Al rich phase in which γ' imbedded is surrounded by the ternary Cu_2MnAl rich phase, so that the mode of $DO_3 \rightleftharpoons \gamma'$ would be restricted by the strain due to the misfit between the Cu_3Al phase and the Cu_2MnAl phase. This may be the reason why the lattice parameters of the γ' phase in the Cu_3Al rich phase differs from those in Cu-Mn-Al or Cu-Al, and why the structure of the phase is close to tetragonal (a = 4.12Å and c = 4.03Å).

The orientation relationship between the $L1_0$ phase (γ' phase) and Cu_2MnAl have been reported as followed:[13]

$$(010)_{L1_0} \parallel (001)_{L2_1}$$
$$[001]_{L1_0} \parallel [110]_{L2_1}$$

This orientation relationship is basically the same as the lattice correspondence explained before. But previous observation of the particles in a [110] foil has shown that the $L1_0$ particles are distributed in platelets lying in the (001) plane of the matrix.[4,13] The present high resolution dark field micrograph shown in Fig. 6(b) reveals, however, that the γ' particles are not elongated along the (001) plane of the

matrix, but rather along the ⟨111⟩ directions of the matrix. The trace analysis of this direction yields the following orientation relationship.

$$(001)_{\gamma'} \parallel (110)_{\beta'} \quad , \quad [\bar{1}11]_{\beta'} \parallel [\bar{2}\bar{1}0]_{\gamma'}$$

$$\text{or } [1\bar{1}1]_{\beta'} \parallel [2\bar{1}0]_{\gamma'}$$

A similar orientation relationship was reported in Cu-Sn martensite.[30] In the Cu-Sn system, two kinds of martensite were observed, banded (β') and wedge-shaped (β''), depending on the heat treatment. The former was found to be an orthorhombic lattice of AB'AC' type with stacking faults in the quenched state. The latter was found to be the orthorhombic lattice of AB' type, which is equivalent to the structure of the γ' phase found in this investigation, when the alloy was subzero-cooled. The orientation relationship obtained in the latter case was $(001)_{\beta''} \parallel (110)_{\beta_2}$ and $[2\bar{1}0]_{\beta''} \parallel [\bar{1}1\bar{1}]_{\beta_2}$, which holds good when the twinning plane is expected as (121) and the stacking fault plane as $(1\bar{2}1)$.

Also in the present investigation the same relationship is found to hold. The particles are lengthened along the (121) or $(\bar{1}\bar{2}1)$ plane and the direction of the streaks in the diffraction pattern is normal to the trace of the (121) or $(\bar{1}\bar{2}1)$ plane. This analysis suggests that the (121) or $(\bar{1}\bar{2}1)$ plane would be the twinning plane or stacking fault plane in the γ' phase.

The γ' martensites shown in Figs. 18 and 19, in the Cu-12.5 wt% Al-4.68 wt% Mn alloy located at the Cu_3Al rich side of the miscibility gap, indicate that oil quenching produces twinning plates (Fig. 18) and furnace cooling gives highly faulted plates (Fig. 19). Figure 19 is very similar to faulted martensite structures observed in binary Cu-Al alloys (e.g., References 16 and 17). Thus, the γ' phase which emerges in the

Cu_3Al rich spinodal product, might have the same features (i.e., internal faulting or twinning). However, the γ' phase of the furnace cooled $Cu_{2.5}Mn_{0.5}Al$ alloy is expected to have a faulted character, since slower quenching results in the faulted structure for the alloy near the end of miscibility gap. The diffuse streaks in the diffraction pattern shown in Fig. 7 may, therefore, be due to the internally faulted structure of the γ' phase.

3. <u>γ' Phase and Spinodal Decomposition</u>

The γ' phase would vary its structure and Ms temperature due to changes in Mn or Al content and heat-treatment. Complications in uniquely identifying the γ' phase arise from the fact that the wavelength (λ) of the sinusoidal composition modulations show strong variation with aging, so that Mn or Al concentration changes with aging inside the miscibility gap.

It has been reported that at the early stages of coarsening,[13] the structure of the binary phase is mostly that of γ' phase. In the intermediate stages of coarsening the volume fraction of the γ' phase within the binary phase decreases by about a factor of 3 between 300 to 3000 min aging. By aging at temperatures above 275°C, the binary phase has mainly the DO_3 structure, with a relative absence of γ' particles.

These observations could be explained by the peudo-binary phase diagram along composition line Cu_3Al-Cu_2MnAl shown in Fig. 1. The composition of the equilibrium phase at the Cu_3Al rich side after aging at 225°C is estimated as Cu-12.5 wt% Mn-4.6 wt% Al from the figure. Since composition itself is responsible for producing the Cu-Mn-Al martensite as seen in Figs. 18 and 19, it is expected that the γ' phase would appear even after long time aging at 225°C. However, 275°C and 325°C

aging for long times (i.e., 10,000 min) would not give rise to the γ' phase, simply because the expected compositions of Cu-Al rich side after long time aging are Cu-12.5 wt% Al-6.12 wt% Mn and Cu-12.6 wt% Al-10.26 wt% Mn respectively. Higher Mn contents tend to depress the Ms temperature.

Moreover, in the early stages of spinodal decomposition, some amount of Mn atoms do not diffuse from the binary rich phase. Consequently in the initial spinodal reaction the Mn concentration in the binary phase would be higher than that at the later stage of aging, so that the γ' phase would not appear within the binary phase. It has been reported that the Cu_3Al rich phase is distorted to a tetragonal symmetry before losing coherency.[3] This tetragonal structure of the Cu_3Al undergoes compression along cubic directions, as set up by the ternary phase. These misfit compression stresses could then be relieved by $\langle 110 \rangle$ shearing if the elastic contant $1/2(C_{11} - C_{12})$, corresponding to $\{110\}\langle 110 \rangle$ shear, would decrease to zero.

Although there is no data about the elastic constant of Cu_3Al, it is expected that lattice softening might occur just before the Ms temperature. This condition might also explain the occurrence of the $DO_3 \rightleftharpoons \gamma'$ transformation, even when the Cu-Al rich phase contains a high Mn content.

V. SUMMARY

The following results and conclusions have been drawn from this investigation:

1. The miscibility gap temperatures of the $(Cu\text{-}Mn)_3Al$ alloy were determined by "in situ" hot stage experiments. The results summarized in Fig. 1 are in agreement with previous studies.

2. The position of the chemical spinodal estimated from the miscibility gap curves, is reinforced by the metallographic observations of the $Cu_{2.5}Mn_{0.5}Al$ and $Cu_{2.2}Mn_{0.8}Al$ alloy in "in situ" experiments. The coherent spinodal curve of the alloys is believed to be in the nearly same position as the chemical spinodal.

3. The APB's in $Cu_{2.5}Mn_{0.5}Al$ developed during aging inherit the same character as those above the miscibility gap, having little interaction with the modulated spinodal structure.

4. The new phase (γ') which emerges within the spinodally transformed Cu-Al rich phase is identified as having an orthorhombic lattice of AB' type, (i.e., two layer stacking $\{110\}_{\beta_1}$ phase) and results from partial transformation of the DO_3 structure.

5. The orientation relationships between the γ' phase and the parent $\beta_1(DO_3)$ phase are

$$(100)_{\beta_1}\ (001)_{\gamma'}\ ,\quad [\bar{1}11]_{\beta_1}\ [\bar{2}\bar{1}0]_{\gamma'}$$

$$\text{or } [1\bar{1}1]_{\beta_1}\ [2\bar{1}0]_{\gamma'}$$

6. The reversion temperature of the γ' phase in furnace cooled $Cu_{2.5}Mn_{0.5}Al$ alloys was determined to be ~205°C by the hot stage work, and his is close to the Ms temperature (240°C) for γ' martensite in a

Cu-13~15% Al alloy. However, the Ms temperature decreases with increasing Mn and Al content.

7. The Cu-12.4% Al-4.68% Mn alloy, which is almost at the end of miscibility gap near the Cu-Al rich phase, shows that oil quenching results in nearly all single phase material, except for small regions of twinned γ' plates (martensite), but furnace cooling yields a high number of densely faulted γ' plates (martensite). This observation is in good agreement with that of the γ' phase in the spinodally decomposed Cu-Al rich phase, because slower quenching gives a high density of γ' phase in the $Cu_{2.5}Mn_{0.5}Al$ alloy.

0 0 0 0 4 2 0 1 6 4 5

ACKNOWLEDGEMENTS

The author is deeply grateful to Professor Gareth Thomas for his guidance, encouragement, unending patience and support during this work. He is indebted to Dr. R. Sinclair and Mr. R. Gronsky for many helpful discussions and for reviewing the manuscript. He is also thankful to Dr. Omer Van der Biest for his help in computer programming.

This research was performed under the auspices of the U. S. Atomic Energy Commission through the Inorganic Materials Research Division of the Lawrence Berkeley Laboratory.

APPENDIX: CALCULATION OF THE VALUES OF THE EXTINCTION DISTANCE (t_o) OF Cu_3Al

The general procedure to obtain extinction distances is discussed with an example by Thomas.[31]

The values of t_o are obtained using the following expression derived by Hirsch et al.:[32]

$$t_o = \frac{\pi V \cos}{\lambda F} = \frac{\pi a_o^3 \cos\theta}{\lambda F}$$

(s = 0 where s is deviation parameter from the exact Bragg reflection) where λ is the wavelength of the incident beam, V is the volume of the unit cell of edge length a_o and F is the structure factor for the unit cell. The structure factors associated with DO_3 type superlattice are given by the following:

$$F_F^{DO_3} = 4(3f_{Cu} + f_{Al})$$

for h, K, ℓ all even and $\left(\frac{h + k + \ell}{2}\right)$ even

$$F_s^{DO_3} = 4(f_{Cu} - f_{Al})$$

for h, K, ℓ all odd, and

for h, K, ℓ all even and $\left(\frac{h + K + \ell}{2}\right)$ odd

where f_{Cu} and f_{Al} are the electron scattering factor of Cu and Al, respectively. The calculated values of f_{Cu} and f_{Al} are listed in Table IV.

Table IV. Atomic scattering amplitudes for electrons f in Å (after the appendix of Ref. 33).

	(111)	(200)	(220)
F_{Cu}	3.47	3.00	2.01
F_{Al}	2.14	1.76	1.11

Thus, for 100 kV electrons ($\lambda = 3.7\times10^{-10}$), and taking $\cos\theta = 1$, t_o of the (111) reflection for Cu_3Al is obtained as follows

$$t_{o(111)} = \frac{3.14\times(5.83\times10^{-8})^3}{3.7\times10^{-10}\times4(3.47 - 2.14)\times10^{-8}}$$

$$\sim 3160\text{Å}$$

$$t_{o(200)} \sim 590\text{Å}$$

$$t_o(222) \sim 3415\text{Å}$$

REFERENCES

1. O. Heusler, Phys. Gesel, 1399 (1903).
2. R. F. West and L. Thomas, J. Inst. Metals 85, 97 (1956-57).
3. M. Bouchard and G. Thomas, Modulated Structures and Coarsening in Ordered $(Cu\text{-}Mn)_3Al$ Alloys, LBL-2294, 1973.
4. M. Bouchard and G. Thomas, Modulated Structures in $(Cu\text{-}Mn)_3Al$ Alloys II. Formation of an $L1_0$ Phase within the Cu_3Al Side Phase, LBL-2295, 1973.
5. M. Bouchard and G. Thomas, Modulated Structures in $(Cu\text{-}Mn)_3Al$ Alloys III. Formation of the γ Phase, LBL-2296, 1973.
6. J. W. Cahn, Trans. Met. Soc. AIME 242, 166 (1968).
7. J. E. Hilliard, Phase Transformations (Amer. Soc. for Metals, 1970), p. 497.
8. M. Murakami, O. Kawano, Y. Murakami and M. Morinaga, Acta Met. 17, 1517 (1969).
9. E. P. Butler and G. Thomas, Acta Met. 18, 347 (1970).
10. R. J. Livak and G. Thomas, Acta Met. 19, 497 (1971).
11. S. D. Dahlgren, Calculation and Measurement of the Yield Stress of Alloys with Coherent Lamellar Microstructures (Ph. D. Thesis), UCRL-16846, May 1966.
12. R. W. Carpenter, Strengthening Effects of Spinodal Decomposition in Gold-Platinum Alloys and the Kinetics of the Reaction (Ph. D. Thesis), UCRL-16609, January 1966.
13. Fereshteh Samimi Mirmirani, Structure and Mechanical Properties of Cu-Mn-Al Alloy (M. S. Thesis), LBL-2598, April 1974.

0 0 0 0 4 2 0 1 6 4 7

14. M. J. Marcinkowski, Electron Microscopy and Strength of Crystals, G. Thomas and J. Washburn, eds. (Interscience, N. Y., 1962), p. 333.

15. M. J. Marcinkowski and N. Brown, Acta Met. 9, 764 (1961).

16. Z. Nishiyama, J. Kakinoki and S. Kajiwara, J. Phys. Soc. Japan 20(7), 795 (1965).

17. P. R. Swann and H. Warlimont, Acta Met. 11, 511 (1963).

18. S. Kajiwara, J. Phys. Soc. Japan 22(3), 795 (1967).

19. S. Sugino, N. Nakanishi and H. Mitani, J. Japan Inst. of Metals 29, 751 (1965).

20. H. Morikawa, K. Shimizu and Z. Nishiyama, Trans. Japan Inst. Met. 8, 145 (1967).

21. H. E. Cook and J. E. Hilliard, Trans. Met. Soc. AIME 233, 142 (1965).

22. J. E. Morral and J. W. Cahn, Acta Met. 19, 1037 (1971).

23. M. V. Dzhibuti and Yu-D. Tyapkin, Soviet Physics-Crystallography 13, 240 (1968).

24. Yu-D. Tiapkin and M. V. Jibuti, Acta Met. 19, 365 (1971).

25. J. Higgins, R. B. Nicholson and P. Wikes, Acta Met. 22, 428 (1974).

26. M. J. Richards and J. W. Cahn, Acta Met. 19, 1263 (1971).

27. L. Kaufman and M. Cohen, Progress in Metal Phys. 7, 165 (1958).

28. Tarora, J. Japan Inst. of Metals 8, 6 (1944); 13, 3 (1949).

29. R. W. Cahn and J. A. Coll, Acta Met. 9, 138 (1961).

30. H. Morikawa, K. Shimizu and Z. Nishiyama, Trans. Japan Inst. Met. 9, 307, 317 (1968).

31. G. Thomas, Transmission Electron Microscopy of Metals (John Wiley and Sons, Inc., New York, 1962).

32. P. B. Hirsh, A. Howie and M. J.Whelan, Phil. Trans. Roy. Soc. A 252, 499 (1960).

33. P. B. Hirsch, et al., eds., Electron Microscopy of Thin Crystals (Butterworth Scientific Publications, London, 1965).

FIGURE CAPTIONS

Fig. 1. The pseudo binary phase diagram along Cu_2MnAl and Cu_3Al (after Bouchard).[3] The temperatures of the miscibility gap obtained in this investigation are illustrated. The chemical spinodal was calculated using $T_c \sim 355°C$ and $C_c \sim 0.65$ from Ref. 21. The Curie temperatures of the quenched alloys were taken from Ref. 13.

Fig. 2. Schematic representation of the ordering sequence during the quenching of the alloy $Cu_{2.5}Mn_{0.5}Al$ (vertically) and its isothermal decomposition (horizontally).

Fig. 3. Bright field micrographs from the alloy $Cu_{2.2}Mn_{0.8}Al$. Showing the gradual increase in the wavelength of the composition modulation parallel to the cube planes and dissolution of the modulated structures.

Fig. 4. Sections of the corresponding (001) diffraction pattern. The figure illustrates the gradual emergence of the well defined satellites and the gradual decrease of the intersatellite spacing to yield diffraction spot streaking. The temperature of the miscibility gap is believed to be around 358°C.

Fig. 5. Dark field micrographs taken with (111) reflection of the alloy $Cu_{2.5}Mn_{0.5}Al$ in (110) orientation. The figure shows that the smoothly curved 1/4a⟨100⟩ APB's have little interaction with the composition modulation even when the specimen temperature exceeds the miscibility gap temperature.

Fig. 6. (a) Bright field micrograph of the alloy $Cu_{2.5}Mn_{0.5}Al$ cooled in the furnace. (b) Dark field micrograph of the same area imaged with the reflection marked N in Fig. 7 showing γ' particle elongation along ⟨111⟩ directions. (c) Dark field micrograph of the same area obtained with the reflection marked M in Fig. 7, showing that M spots are not due to the Cu-Al rich transformation.

Fig. 7. (110) corresponding diffraction pattern of Fig. 6. The extra reflections marked M are indexed in terms of the proposed γ' phase structure.

Fig. 8. (a) Bright field micrograph of the alloy $Cu_{2.5}Mn_{0.5}Al$ aged at 275°C for 1,000 min, showing the γ' phase imbedded in the Cu_3Al rich phase. (b) Dark field micrograph of the same area imaged with the spot marked N in the corresponding diffraction pattern shown in Fig. 9. The γ' particles are elongated along ⟨133⟩ directions. (c) Dark field micrograph obtained using the reflection marked M in Fig. 9.

Fig. 9. The corresponding (310) diffraction pattern of Fig. 8. Symbols are the same as in Fig. 7.

Fig. 10. (a) Crystal structure of the matrix DO_3 type (β_1). (b) The proposed orthorhombic structure of the γ' phase, showing the lattice correspondence in the transformation from the β_1 matrix to the γ' phase.

Fig. 11. Reciprocal lattice section of the proposed γ' phase, with the calculated structure factors.

Fig. 12. Stereographic projection, showing the orientation relationships between β_1 matrix and γ' phase. Marks □ and ● correspond to the main lattice planes of the β_1 matrix and the γ' phase, respectively. Marks ● indicate those of the γ' phase expected from the assumption that $(001)_{\gamma'} \parallel (110)_{\beta_1}$, $[2\bar{1}0]_{\gamma'} \parallel [1\bar{1}1]_{\beta_1}$. Marks ○ indicate those when the second orientation relationship is assumed to be $[\bar{2}\bar{1}0]_{\gamma'} \parallel [\bar{1}11]_{\beta_1}$.

Fig. 13. A sequence of dark field micrographs of the γ' phase in the furnace cooled $Cu_{2.5}Mn_{0.5}Al$ alloy, imaged with the γ' reflection, indicating the stability of the γ' phase. (g) is the dark field micrograph obtained using the reflection marked M in Fig. 14.

Fig. 14. The corresponding diffraction patterns for the Fig. 13. The reflections due to the γ' phase disappeared around 205°C.

Fig. 15. (a) The bright micrograph of the oil quenched $Cu_{2.2}Mn_{0.8}Al$ alloy aged at room temperature for two months. The foil yields a general morphology which may be due to contamination.
(b) The dark field micrograph imaged with the reflection marked M in the diffraction pattern shown in (c). (c) The corresponding (110) diffraction pattern, showing no γ' spots, but strong M spots.

Fig. 16. The energy of mixing vs composition of various states on the bcc structure from Ref. 26, indicating that an Fe_3Al (Fm3m) type is in the ground state up to 25% B, but a $F\bar{4}3m$ structure is in the ground state between 25 and 50% B.

Fig. 17. Bright field micrograph from the oil quenched Cu-12.4% Al-4.68% Mn alloy in an (001) orientation, showing a large extend of ordered $\beta_1(DO_3)$ single phase.

Fig. 18. Bright and dark field micrographs from the oil quenched Cu-12.4% Al-4.68% Mn alloy, indicating regions containing twinned plate.

Fig. 19. Bright field micrograph from the furnace cooled Cu-12.4% Al-4.68% Mn alloy in and (010) orientation, showing two variants of plates with internal striations. The diffraction patterns (a), (b) and (c) were taken from the corresponding area marked (a), (b) and (c) in the bright field micrograph. The streaks are normal to the striations in the plates are are believed to be due to stacking faults within the plates.

Fig. 20. (001) diffraction pattern of the furnace cooled $Cu_{2.5}Mn_{0.5}Al$ alloy, indexed in terms of the two variants of the γ' phase. The symbols are the same as in Fig. 7.

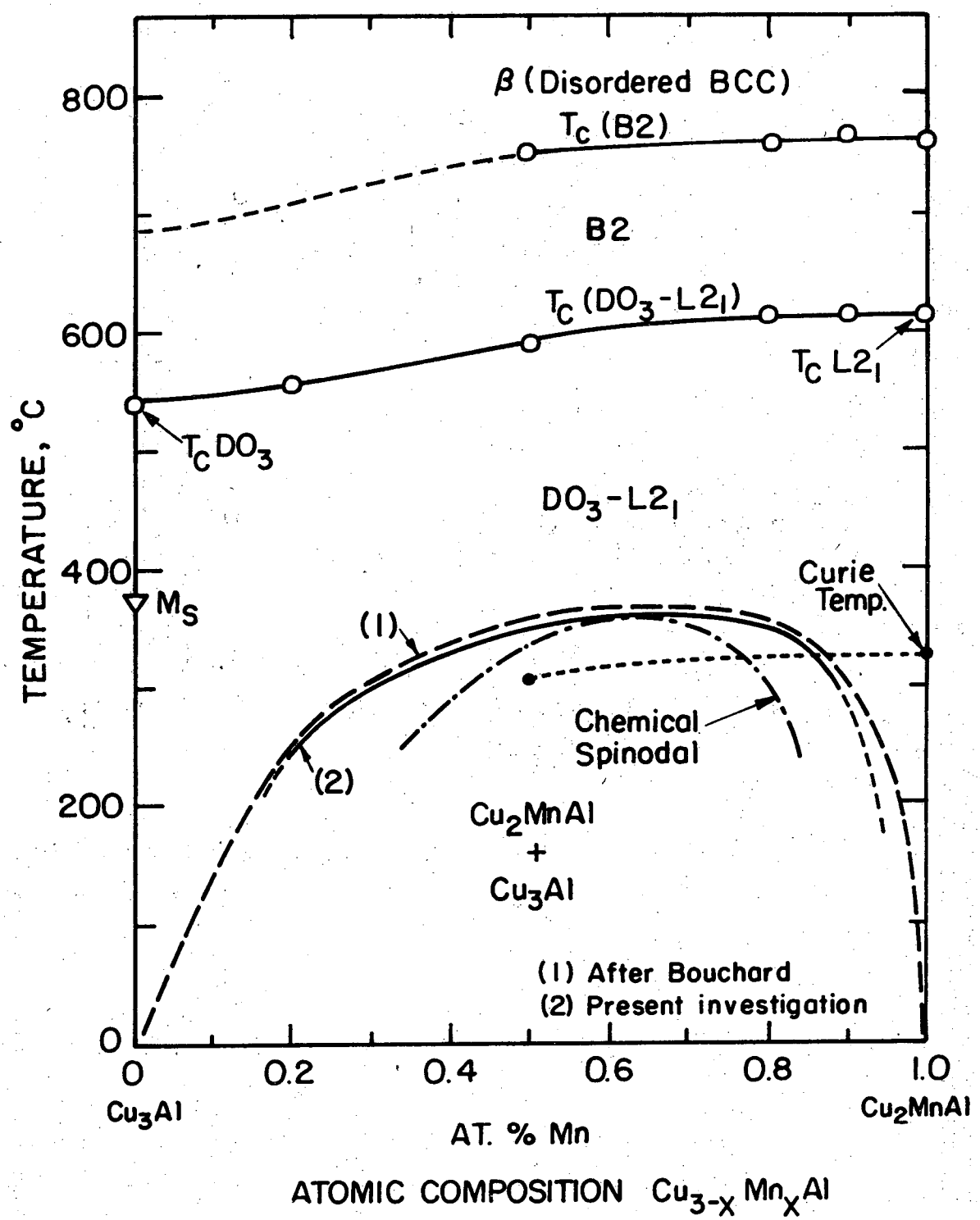

XBL749-7148

Fig. 1

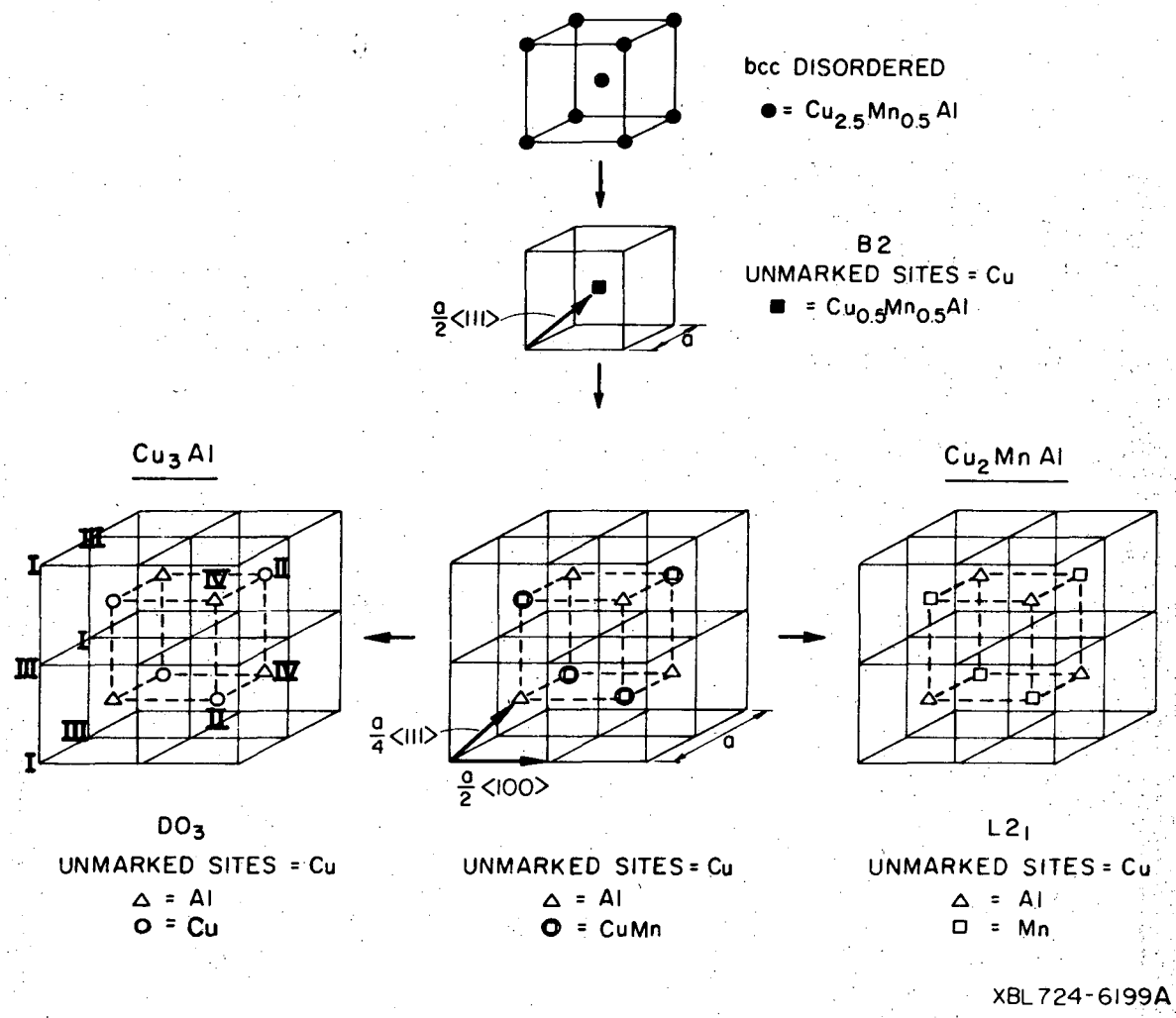

XBL 724-6199A

Fig. 2

0 0 0 0 4 2 0 1 6 5 1

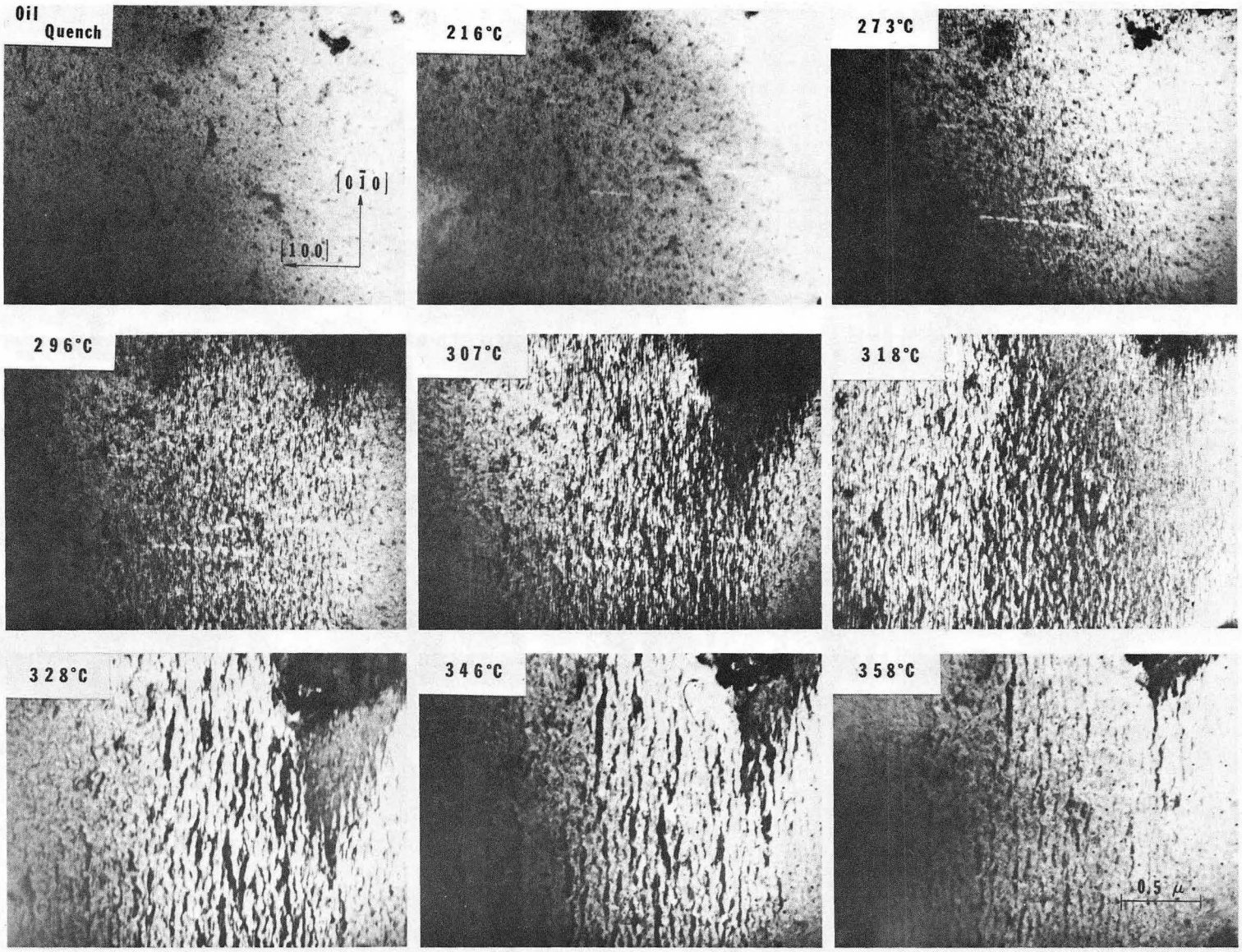

XBB 748-5435

Fig. 3

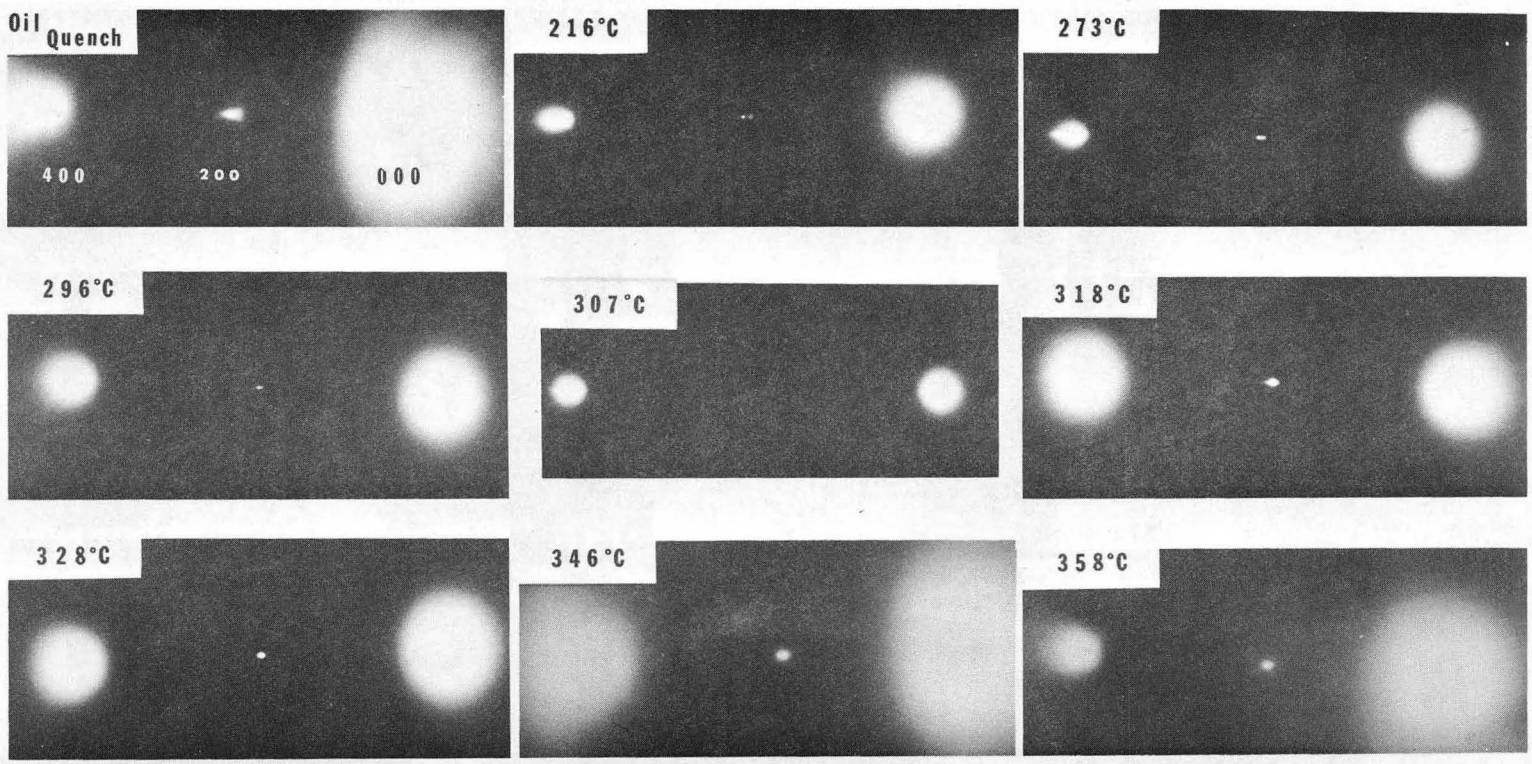

XBB 748-5437

Fig. 4

0 0 0 0 4 2 0 1 6 5 2

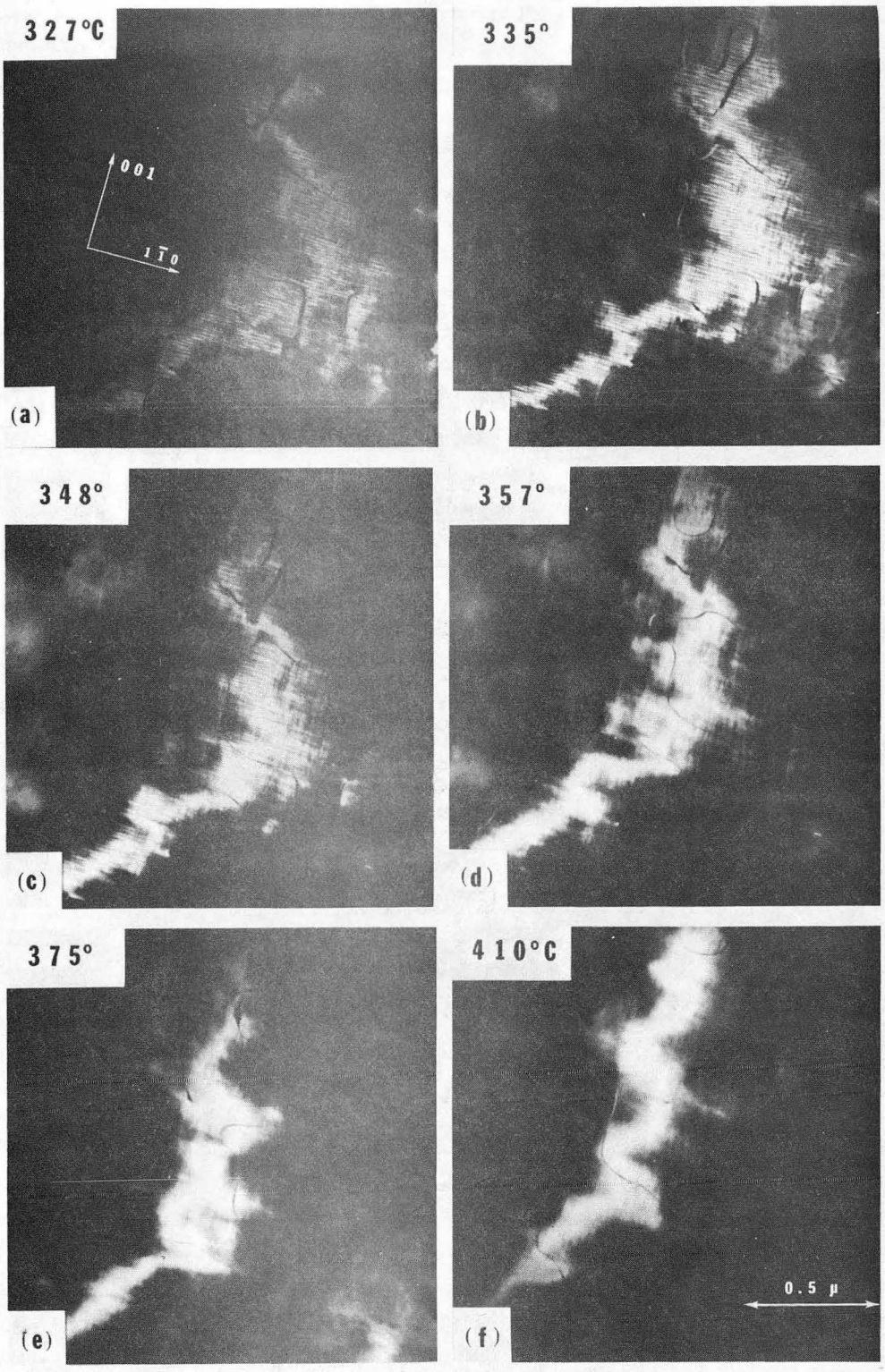

XBB 748-5439

Fig. 5

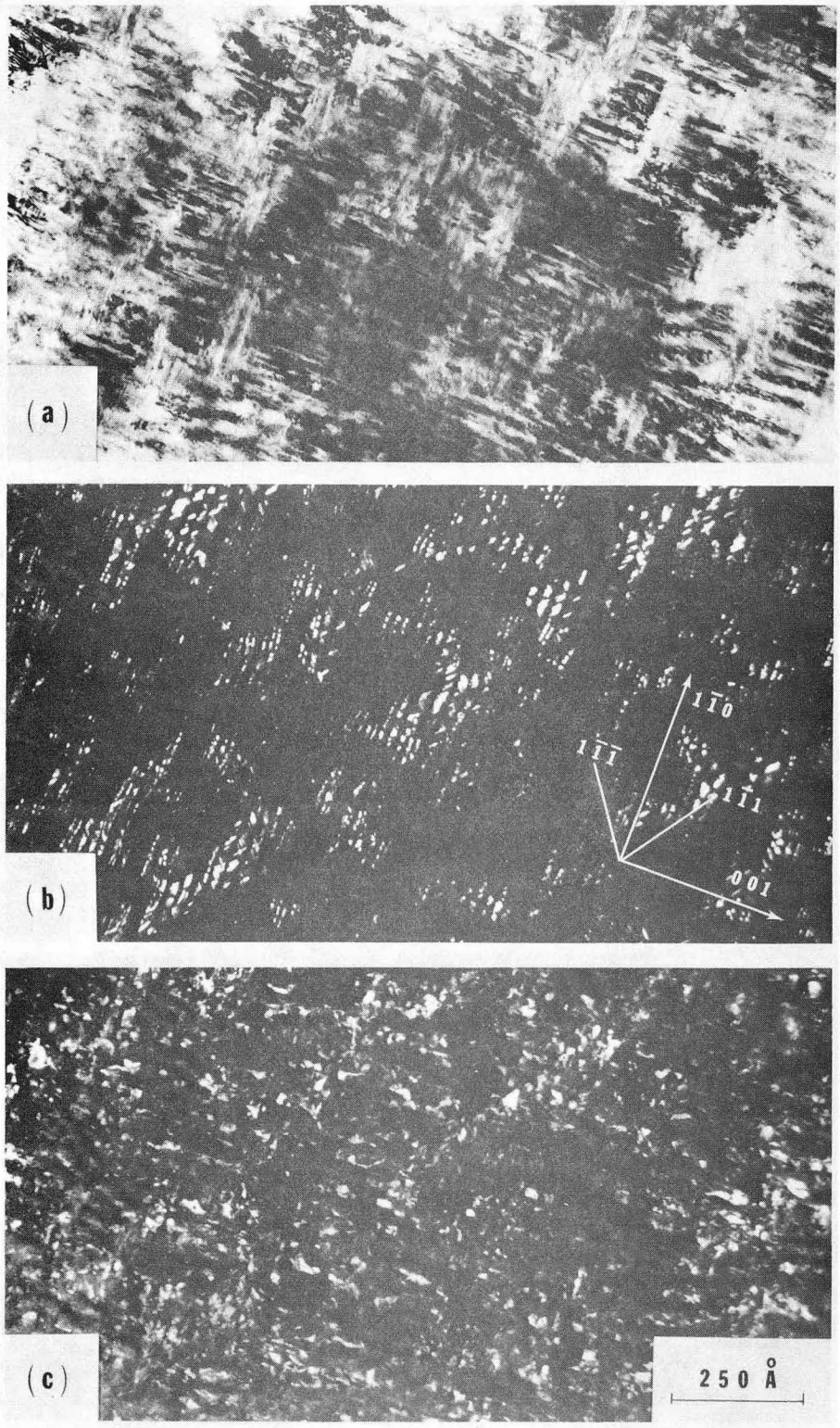

XBB 748-5436

Fig. 6

0 0 0 0 4 2 0 1 6 5 3

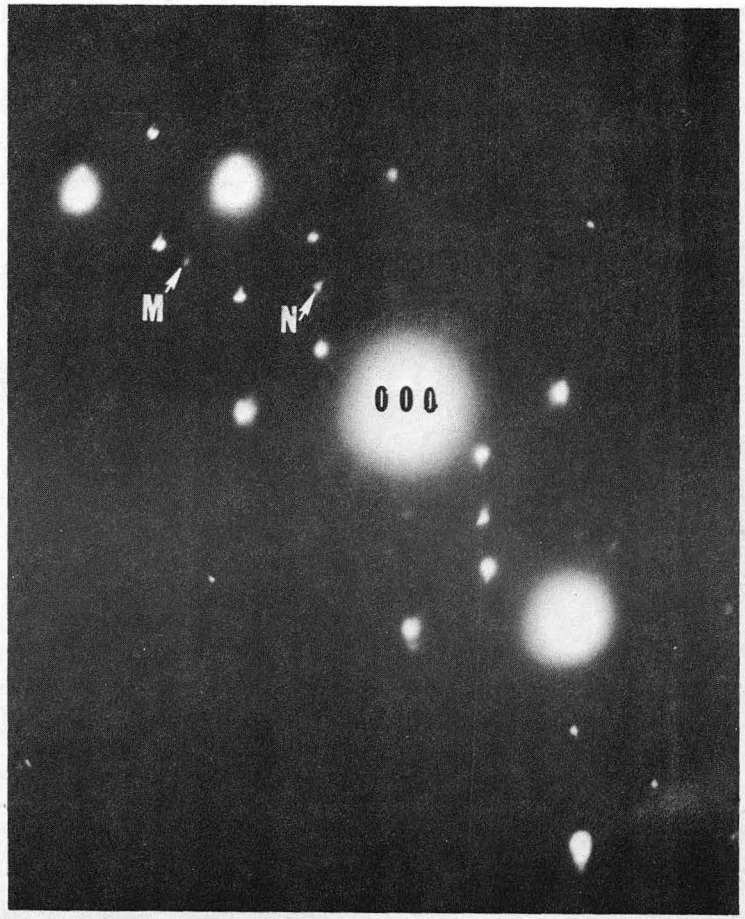

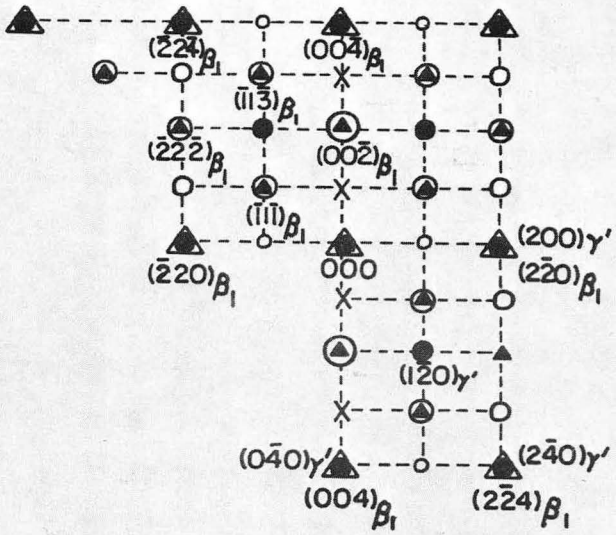

$[110]_{\beta_1} \,//\, [001]_{\gamma'}$

DO_3	△	FUNDAMENTAL
(β_1)	▲	SUPERLATTICE
γ'	●	FUNDAMENTAL
	○	SUPERLATTICE
	X	DOUBLE REFLECTION

XBB 748-5443

Fig. 7

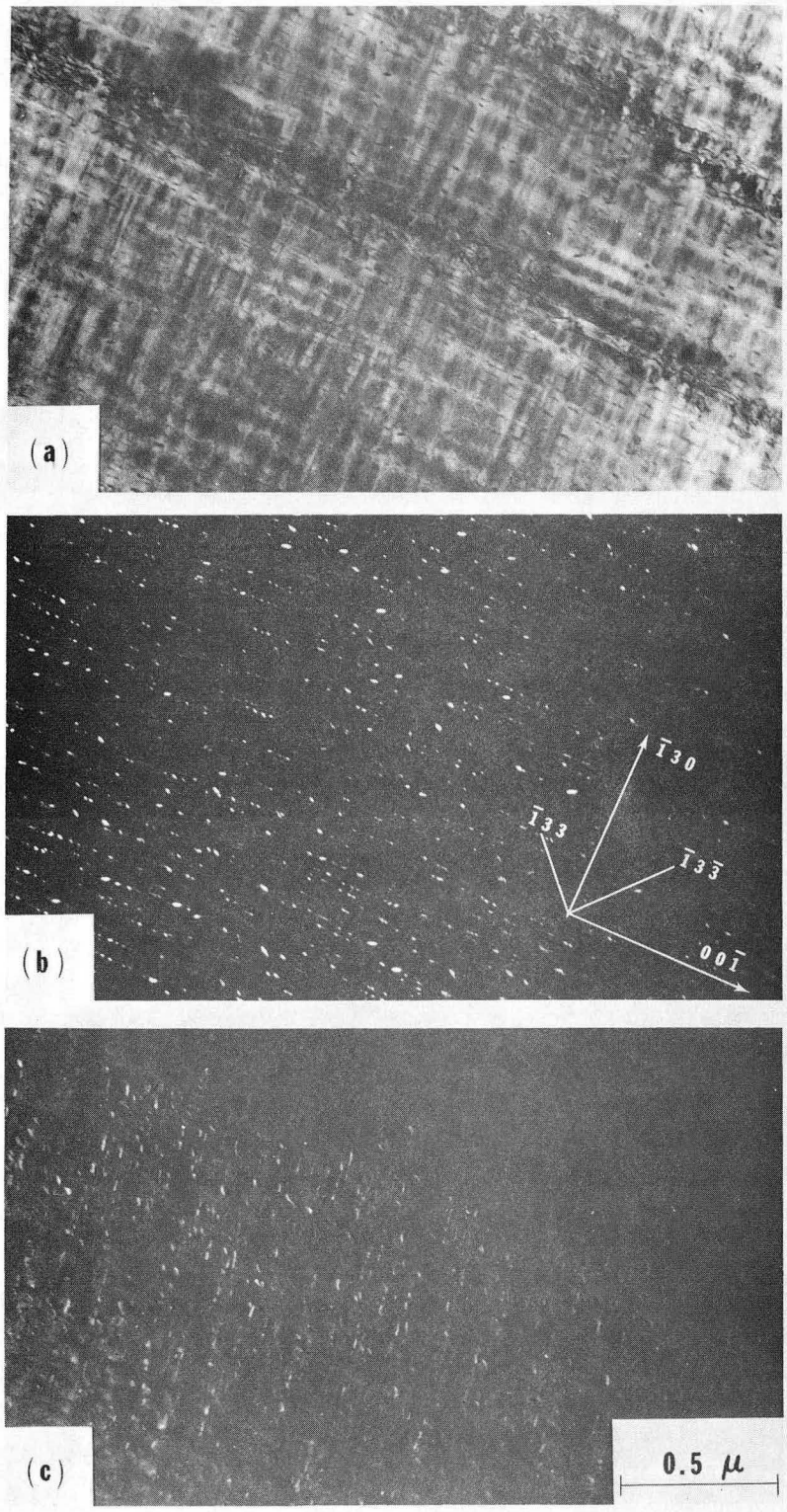

XBB 748-5438

Fig. 8

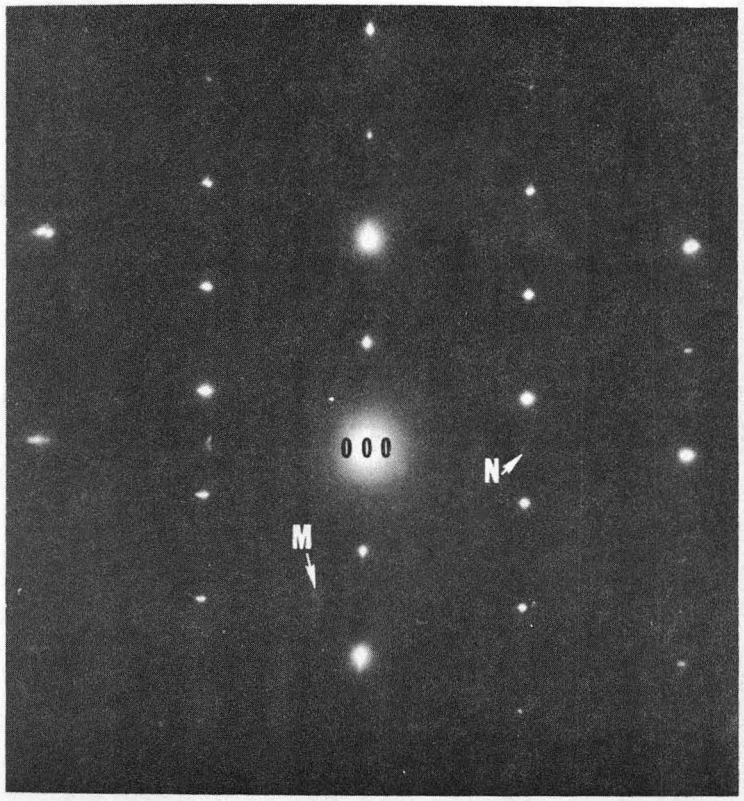

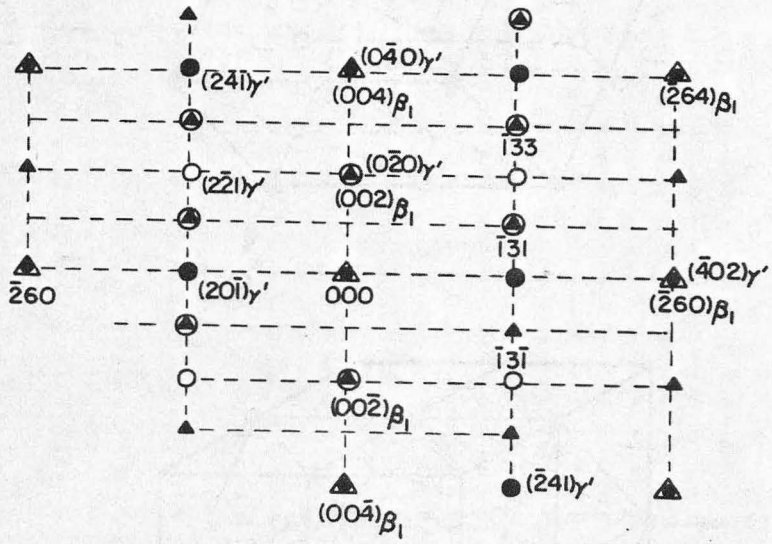

$[310]_{\beta_1} \parallel [102]_{\gamma'}$

XBB 748-5441

Fig. 9

0 0 0 0 4 2 0 1 6 5 4

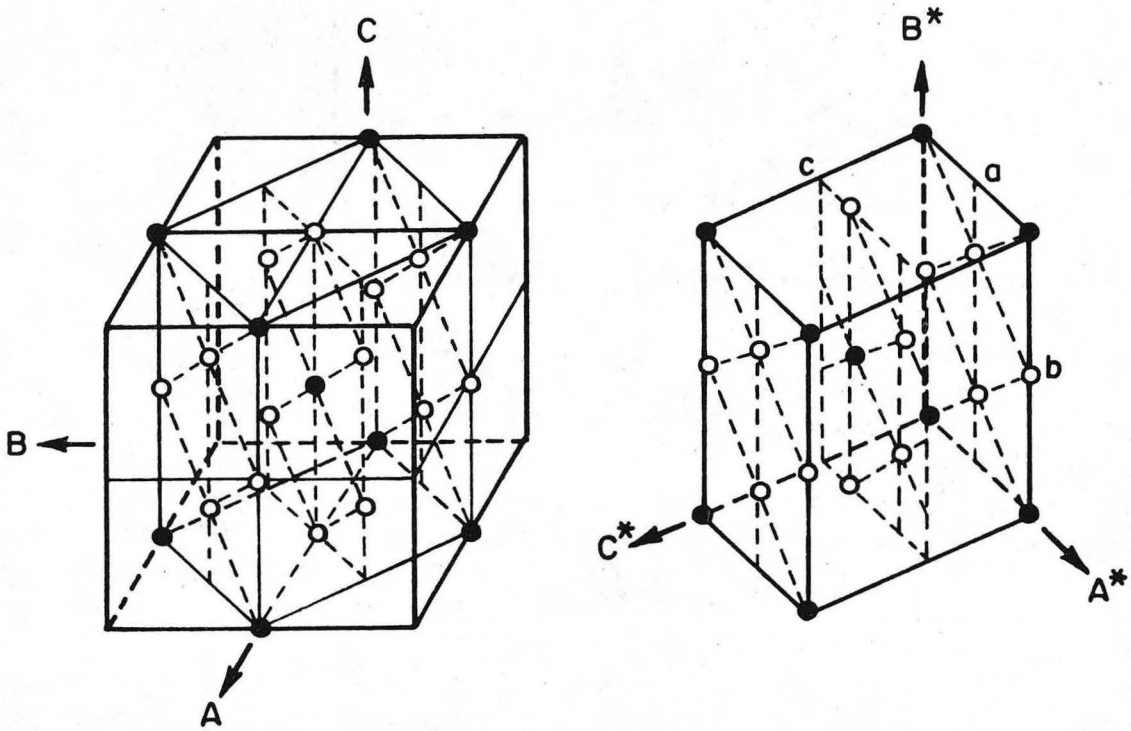

(a) (b)

Cu_3Al (DO_3) ORTHORHOMBIC STRUCTURE

● Al ATOMS
○ Cu ATOMS

XBL 748-6525

Fig. 10

0 0 0 0 4 2 0 1 6 5 5

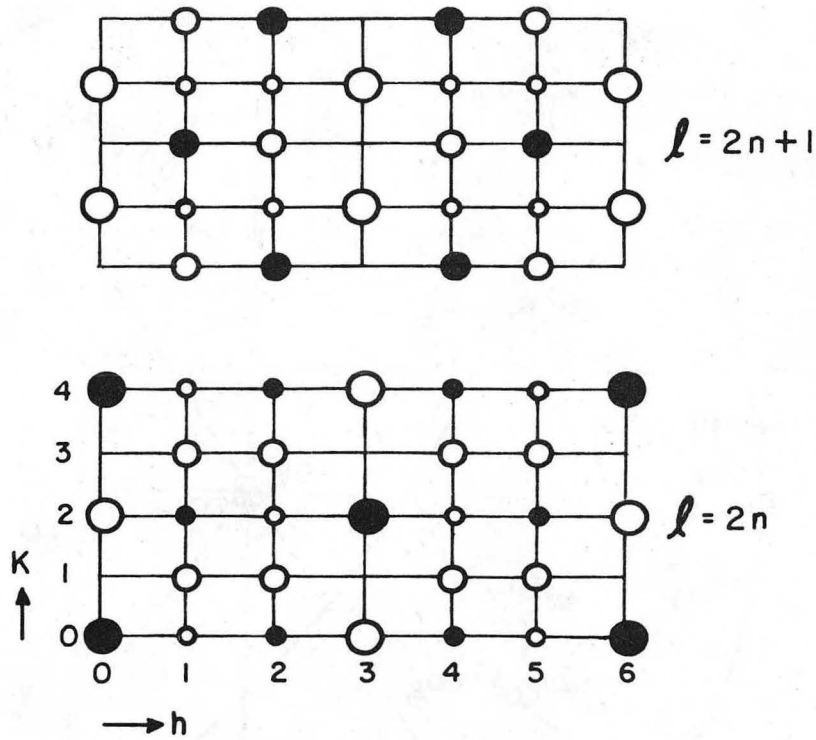

	FUNDAMENTAL		SUPERLATTICE
●	$2(3f_{Cu}+f_{Al})$	○	$2(f_{Cu}-f_{Al})$
●	$\sqrt{3}\,(3f_{Cu}+f_{Al})$	○	$\sqrt{3}\,(f_{Cu}-f_{Al})$
•	$3f_{Cu}+f_{Al}$	∘	$f_{Cu}-f_{Al}$

XBL 748-6528

Fig. 11

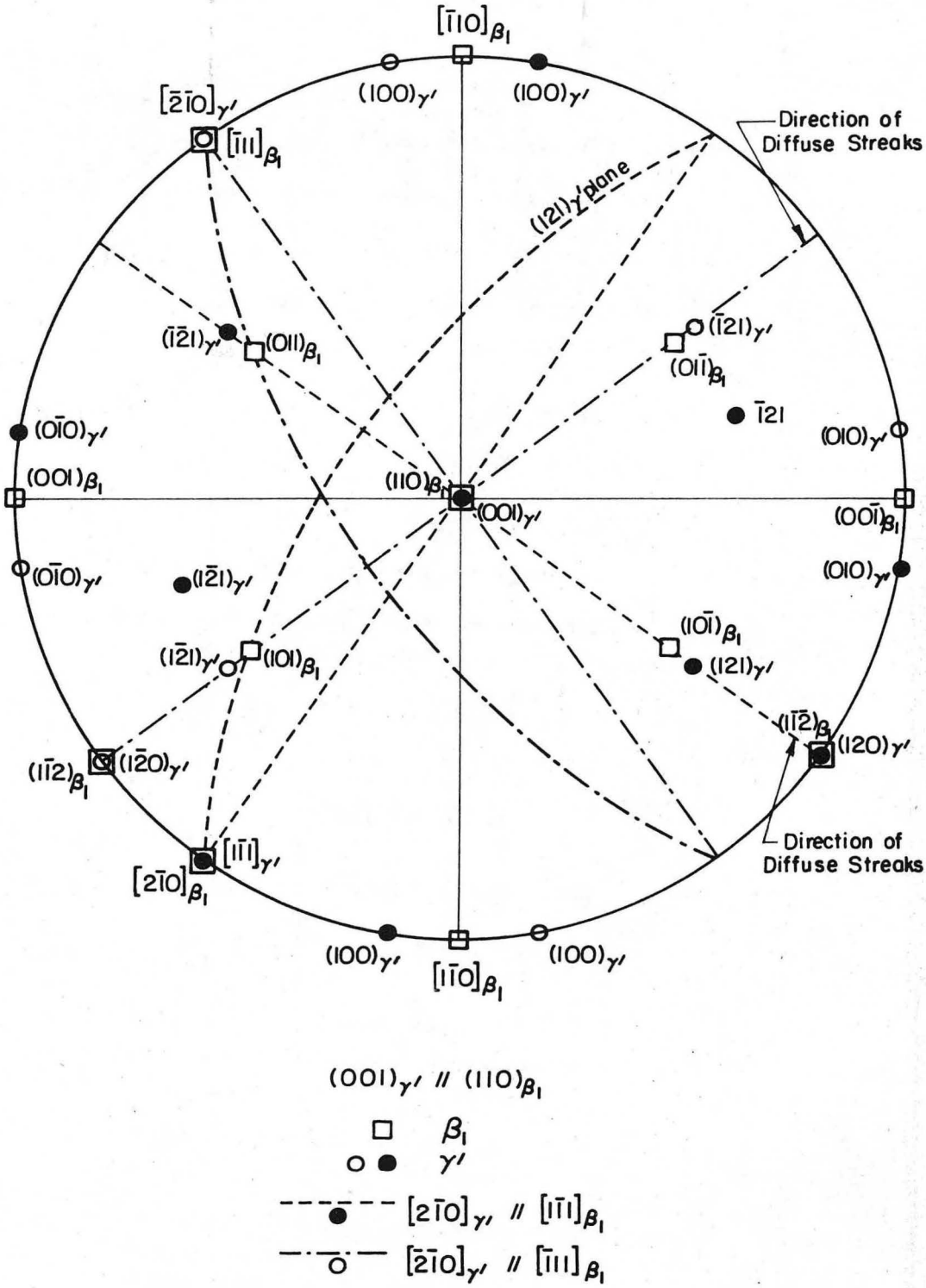
$[\bar{1}10]_{\beta_1}$
$(100)_{\gamma'}$
$(100)_{\gamma'}$
$[\bar{2}\bar{1}0]_{\gamma'}$
$[\bar{1}11]_{\beta_1}$
Direction of Diffuse Streaks
$(121)_{\gamma'}$ plane
$(\bar{1}\bar{2}1)_{\gamma'}$
$(011)_{\beta_1}$
$(\bar{1}21)_{\gamma'}$
$(01\bar{1})_{\beta_1}$
$\bar{1}21$
$(0\bar{1}0)_{\gamma'}$
$(010)_{\gamma'}$
$(001)_{\beta_1}$
$(110)_{\beta_1}$
$(001)_{\gamma'}$
$(00\bar{1})_{\beta_1}$
$(0\bar{1}0)_{\gamma'}$
$(1\bar{2}1)_{\gamma'}$
$(010)_{\gamma'}$
$(10\bar{1})_{\beta_1}$
$(1\bar{2}1)_{\gamma'}$
$(101)_{\beta_1}$
$(121)_{\gamma'}$
$(1\bar{1}\bar{2})_{\beta_1}$
$(120)_{\gamma'}$
$(1\bar{1}2)_{\beta_1}$
$(1\bar{2}0)_{\gamma'}$
Direction of Diffuse Streaks
$[1\bar{1}1]_{\gamma'}$
$[2\bar{1}0]_{\beta_1}$
$(100)_{\gamma'}$
$[1\bar{1}0]_{\beta_1}$
$(100)_{\gamma'}$
$(001)_{\gamma'} \parallel (110)_{\beta_1}$
β_1
γ'
$[2\bar{1}0]_{\gamma'} \parallel [1\bar{1}1]_{\beta_1}$
$[\bar{2}\bar{1}0]_{\gamma'} \parallel [\bar{1}11]_{\beta_1}$
XBL749-7147

Fig. 12

0 0 0 0 4 2 0 1 6 5 6

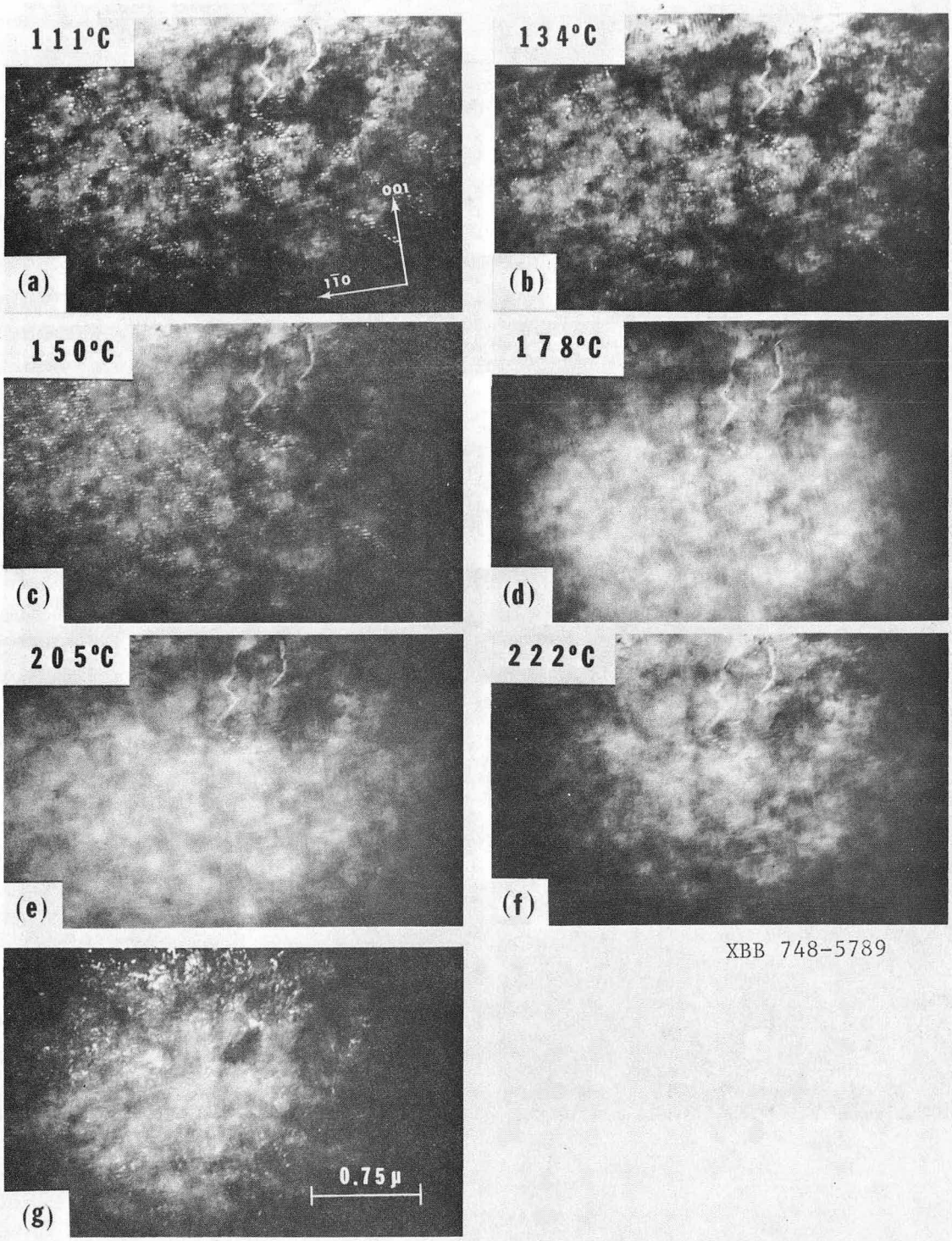

XBB 748-5789

Fig. 13

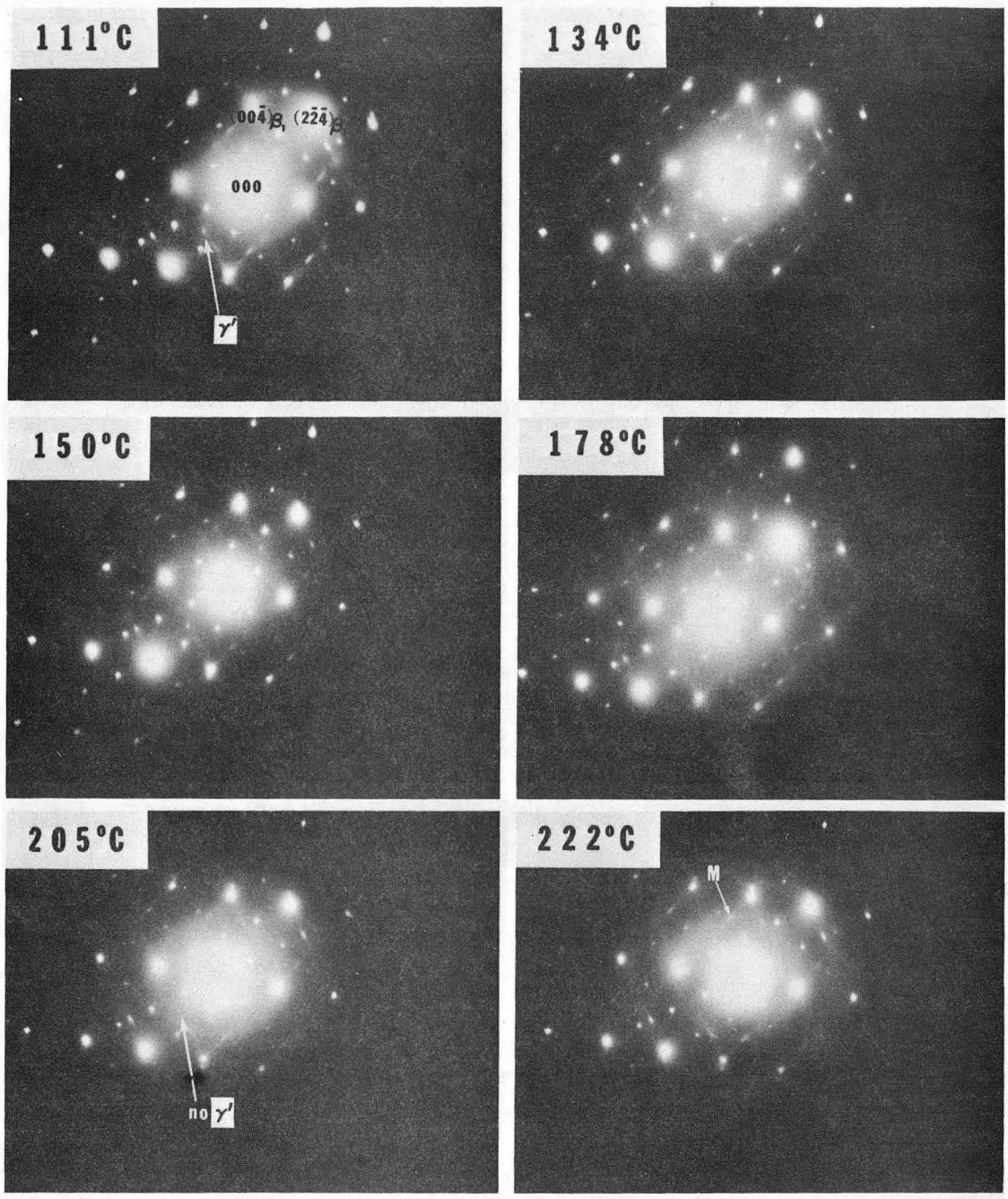

XBB 748-5787

Fig. 14

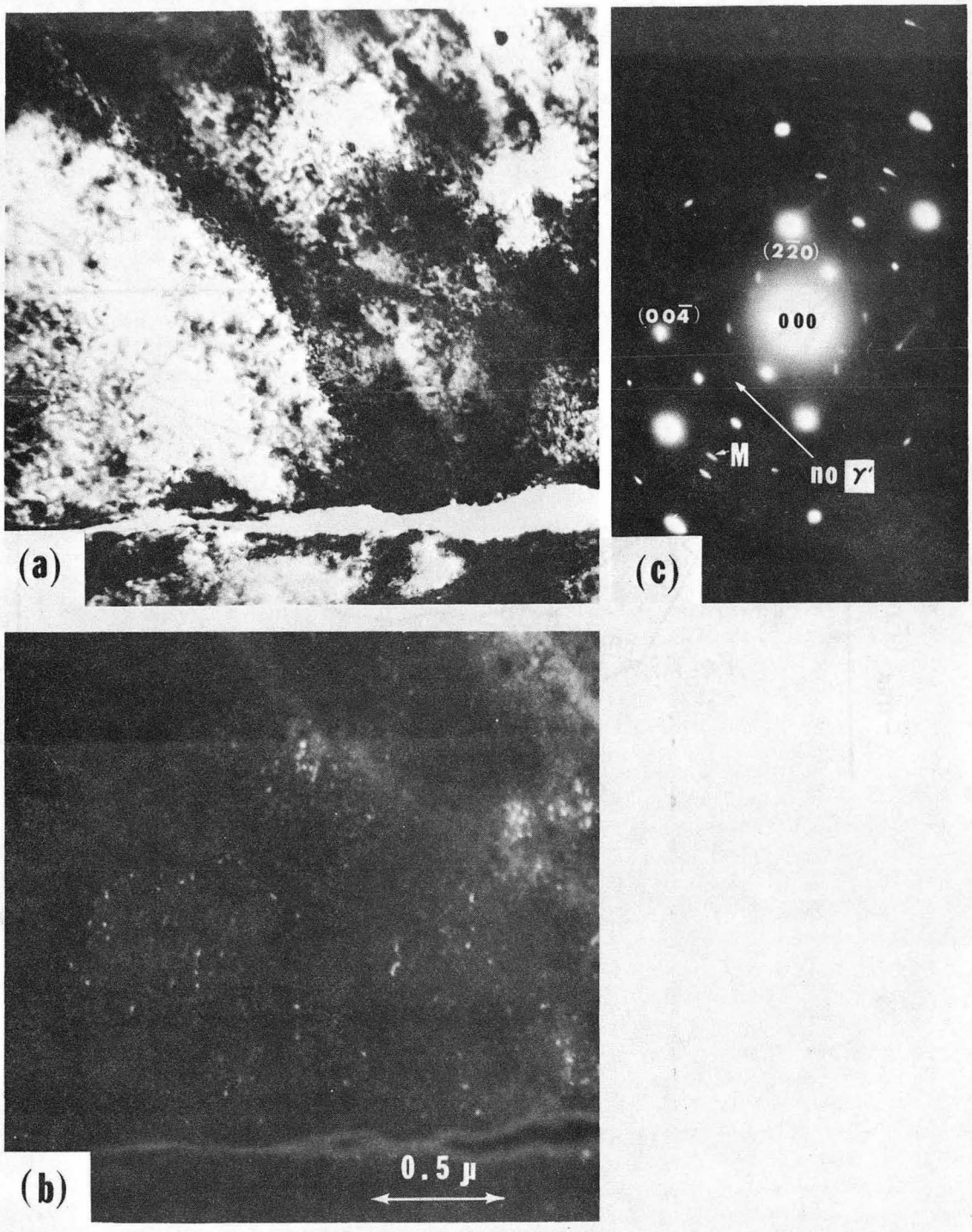

XBB 748-5788

Fig. 15

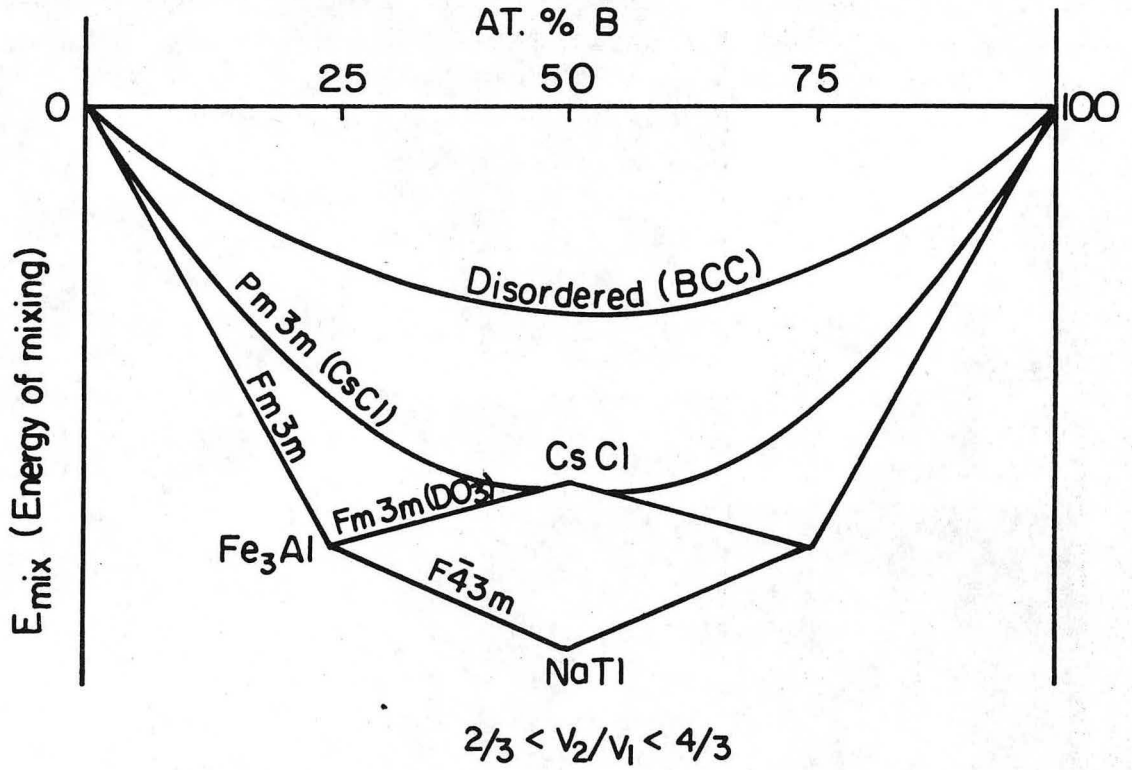

XBL 749-7149

Fig. 16

0 0 0 0 4 2 0 1 6 5 7

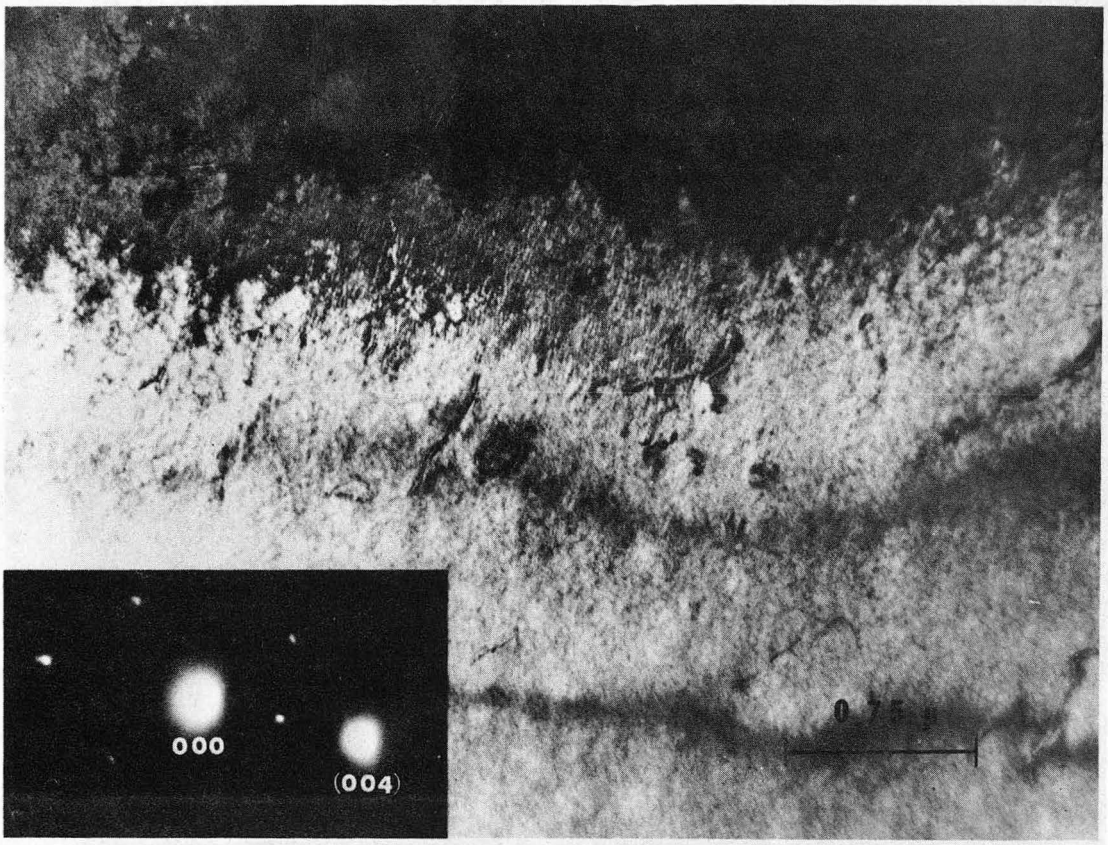

XBB 748-5785

Fig. 17

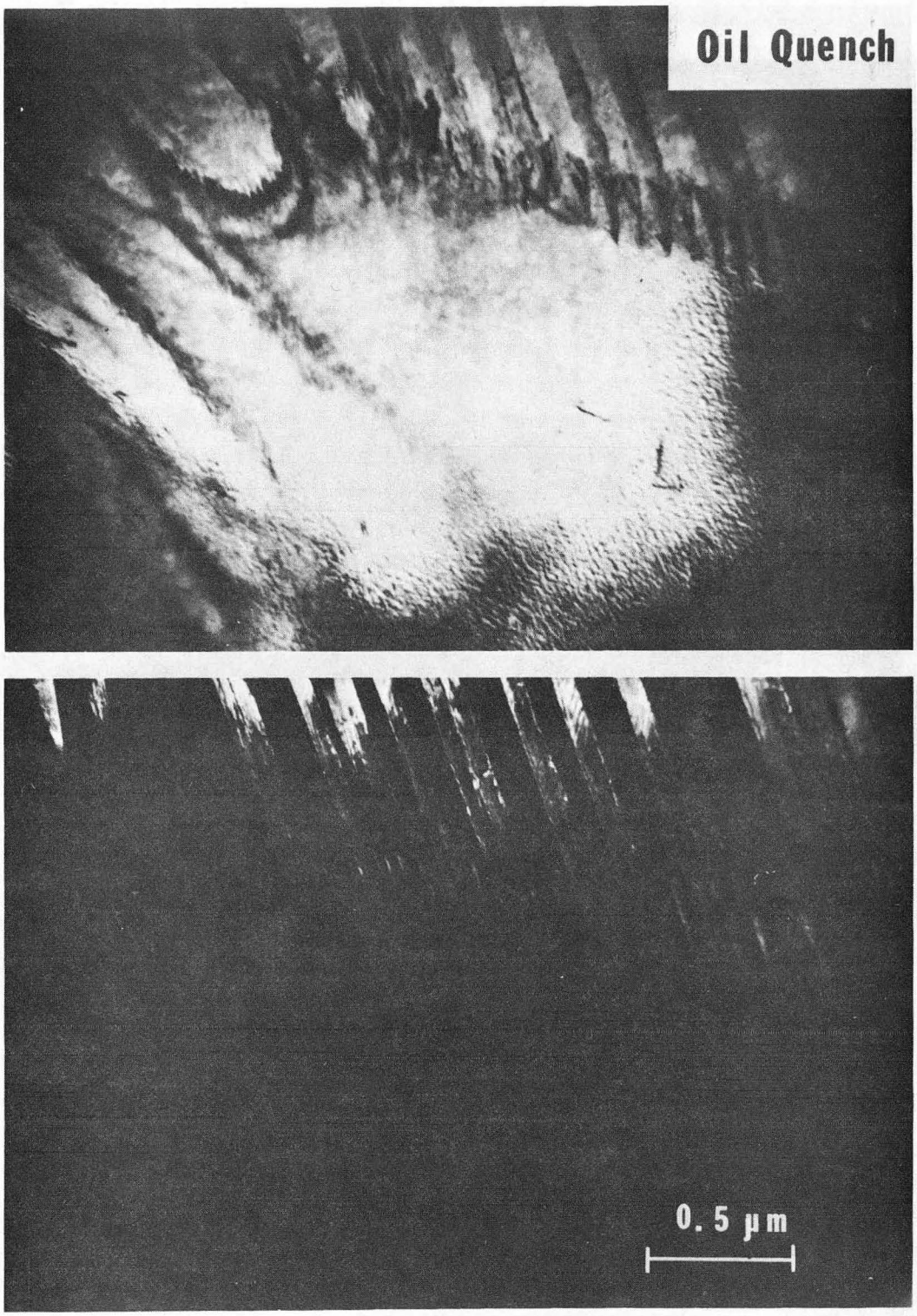

XBB 749-6114

Fig. 18

0 0 0 0 4 2 0 1 6 5 8

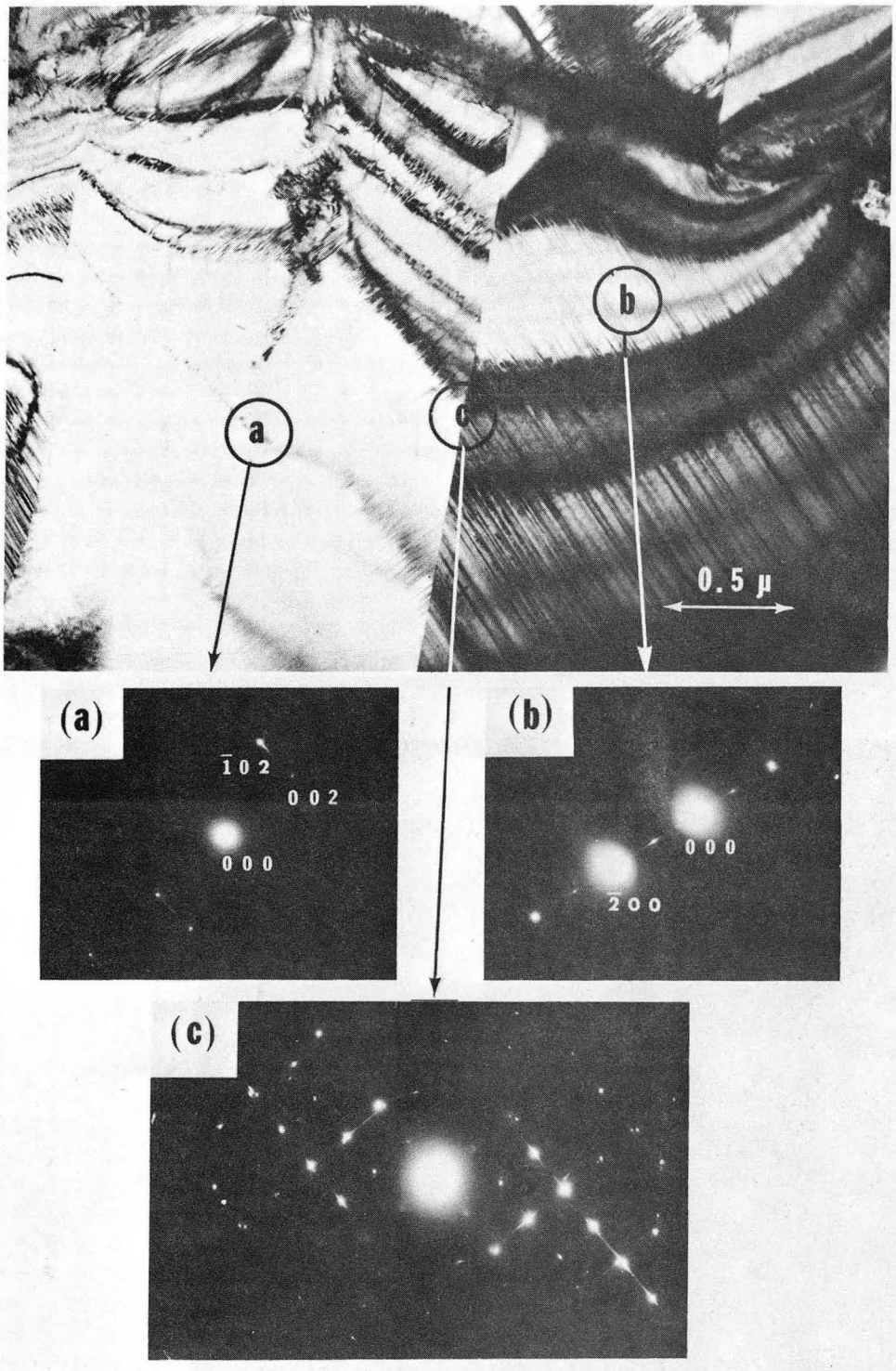

XBB 748-5786

Fig. 19

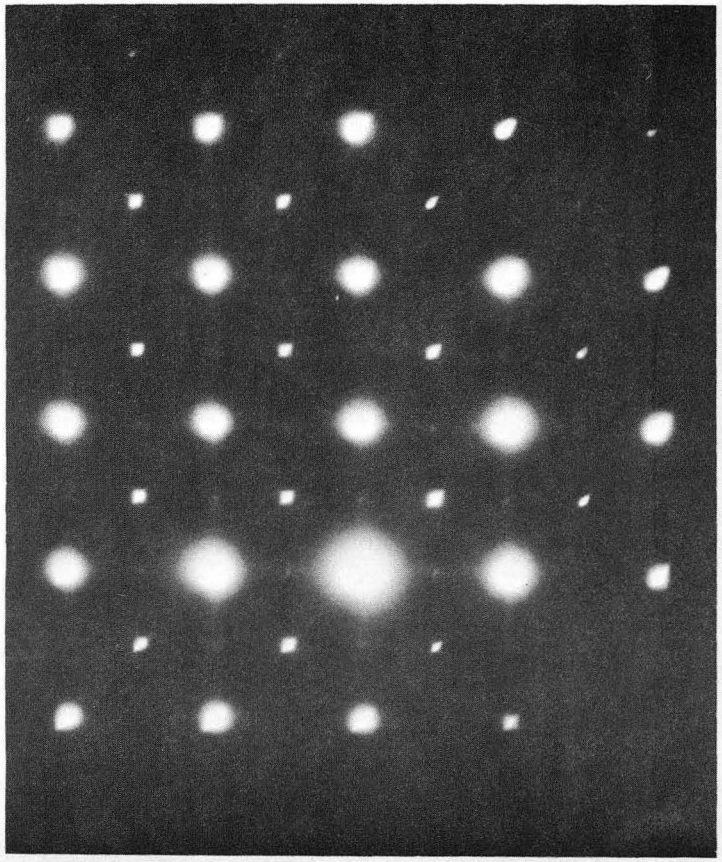

XBB 748-5440

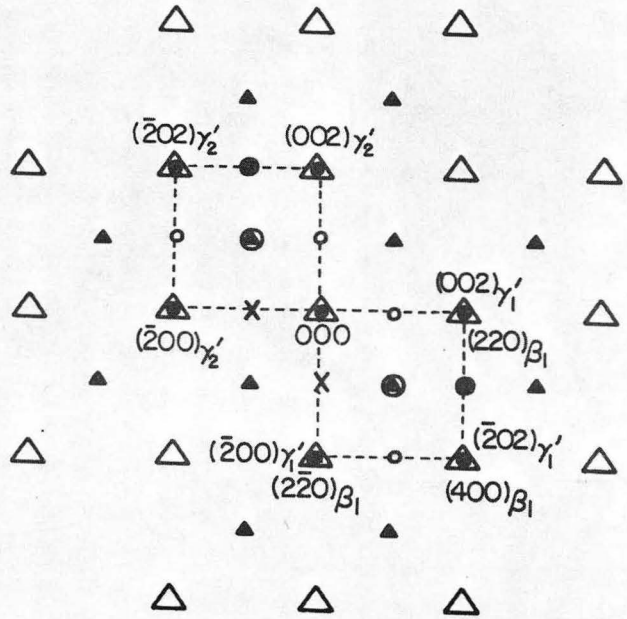

$[00\bar{1}]_{\beta_1} \parallel [010]_{\gamma'}$

Fig. 20

0 0 0 0 4 2 0 1 6 5 9

LEGAL NOTICE

This report was prepared as an account of work sponsored by the United States Government. Neither the United States nor the United States Atomic Energy Commission, nor any of their employees, nor any of their contractors, subcontractors, or their employees, makes any warranty, express or implied, or assumes any legal liability or responsibility for the accuracy, completeness or usefulness of any information, apparatus, product or process disclosed, or represents that its use would not infringe privately owned rights.

TECHNICAL INFORMATION DIVISION
LAWRENCE BERKELEY LABORATORY
UNIVERSITY OF CALIFORNIA
BERKELEY, CALIFORNIA 94720